FABRICATION AND CHARACTERIZATION OF SINTERED RECYCLED GLASS DESIGNED FOR POLLUTED SOIL FILTERING

By
Wesley Cuadrado Castillo

A thesis submitted in partial fulfillment of the requirements for the degree of

MASTER OF SCIENCE
In
MECHANICAL ENGINEERING

UNIVERSITY OF PUERTO RICO
MAYAGUEZ CAMPUS

July 2014

Approved by:

_____	_____
O. Marcelo Suárez, Ph.D. President, Graduate Committee	Date
_____	_____
Rubén Díaz, Ph.D. Member, Graduate Committee	Date
_____	_____
Ricky Valentín, Ph.D. Member, Graduate Committee,	Date
_____	_____
Ricky Valentín, Ph.D. Chairperson of the Department	Date
_____	_____
Ricardo R. López Rodríguez, Ph.D. Graduate School Representative	Date

Abstract

Soil pollution generates diseases, hunger, and agricultural problems. Porous recycled glass beds were produced to study the feasibility of using them for polluted soil filtering. This research discusses structural and mechanical parameters of filters made from commercially available powdered recycled glass. M30 and MG80 powdered recycled glass were sintered from 700ºC to 800ºC at different times. Porosity and percolation characteristics were studied according to changes in sintering parameters and MG30-MG80 mixture ratios. Moreover, since TiO_2 can serve as a photocatalyst to degrade soil pollutants, the effects of adding TiO_2 to recycled glass powders were also studied. Resulting porous glass specimens were characterized by optical microscopy and their porosity assessed by quantitative image analysis. Additionally, samples percolation was determined by recording the elapsed time to obtain a water volume change of 600 ml. Finally, we obtained a map that specifies recycled glass filter's porosity, percolation, and compression characteristics according to sintering time, sintering temperature, glass particle size, and the percentage of TiO_2 added.

Resumen

La contaminación en suelos genera enfermedades, hambre y problemas agrícolas. En este trabajo de investigación, filtros de vidrio reciclado fueron producidos para estudiar la viabilidad de su uso para el filtrado de suelos contaminados. Esta investigación analizará los parámetros estructurales y mecánicos de los filtros. Polvos de vidrio reciclado M30 (tamaño promedio de partícula de 0.60 mm) y MG80 (tamaño promedio de partícula de 0.18 mm) fueron sinterizados de 700ºC a 800ºC por diferentes tiempos. Características estructurales, como porosidad y percolación, fueron estudiadas de acuerdo a cambios en parámetros de sinterizado y de mezclas de MG30 + MG80. Además, se estudiaron los efectos de la adición de TiO_2 a los polvos de vidrio reciclado. El dióxido de titanio (TiO_2) servirá como el agente foto - catalizador que degradará los contaminantes del suelo. Los especímenes resultantes de vidrio poroso se caracterizaron por microscopía óptica y su porosidad fue evaluada mediante análisis de imagen cuantitativo. Por otra parte, la percolación de agua a través de las muestras se determinó registrando el tiempo transcurrido para obtener un cambio de volumen de agua de 600 ml. Finalmente, se obtuvo un mapa que especifica la porosidad del filtro de vidrio reciclado, la percolación, y las características de compresión de acuerdo con el tiempo y temperatura de sinterizado, tamaño de partícula de vidrio, y el porcentaje de TiO_2 añadido.

Acknowledgements

This project and its participants have been financially supported by the Center for Education and Training in Agriculture and Related Sciences (CETARS) of the University of Puerto Rico-Mayaguez through grant Nº 2011-38422-30835 from the US National Institute of Food and Agriculture. Additional material is based upon work partially supported by the National Science Foundation under Grant HRD 0833112 (CREST program).

I would like to recognize the support of my family, friends, and co-workers, especially Liliana M. Hernández, Gerardo A. Nazario, and Jorge De Jesús, that helped me with the fulfillment of this great research. Special thanks to Dr. O. Marcelo Suárez and Dr. Félix Román, professors at the University of Puerto Rico at Mayagüez, for giving me the opportunity to grow academically and professionally.

Table of Contents

Abstract ii

Resumen iii

Acknowledgements iv

List of Tables xv

List of Figures xv

List of Symbols xix

List of Abbreviations xx

Chapter 1 Background

1.1. Introduction 1

1.2. Soil Pollution 2

1.3. Soil Remediation Systems 4

1.3.1. Soil Vapor Extraction 4

1.3.2. Soil Washing 5

1.4. Ground Water Pollution 5

1.5. Ground Water Remediation Systems 7

1.5.1. Pump and Treat Remediation System 7

1.5.2. Air Sparging 8

1.5.3. Permeable Reactive Barriers 9

1.6. Glass Recycling 10

1.7. Sintering 12

1.7.1. Solid-state sintering 12
1.7.2. Viscous Sintering 14
1.7.3. Grain Growth in Porous Media 15

Chapter 2 Problem Statement

2.1 Main Idea 16
2.2 Design Criteria 16
2.3 Materials Specifications 17
2.3.1. Recycled Glass Powder 17
2.3.2. TiO_2 Particles 17
2.3.3. X-Ray Diffraction 18
2.3.4. Thermogravimetric Analysis (TGA) 20

Chapter 3: Pollutant Degradation

3.1. Photocatalytic Activity 21
3.1.1. Introduction 21
3.1.2. Fundamentals of photocatalytic reactions 23
3.2. Recycled Glass Powder Surface Functionalization 24
3.2.2. Methodology 24
3.2.2.1. Recycled glass and titanium (IV) oxide anhydrous powder 24
3.2.2.2. Heterogeneous Nucleation Method 25
3.2.2.2.1. Recycled Glass Pretreatment 25
3.2.2.2.2. Synthesis of TiO_2 Nanoparticles + Glass Beads 25

3.2.3. Results 26
3.2.3.1. Scanning Electron Microscope (SEM) 26
3.2.3.1.1. MG30, ethanol, and TiO_2 mixtures 26
3.2.3.1.2. MG80, ethanol, and TiO_2 mixtures 27
3.2.3.1.3. Synthesis of TiO_2 Nanoparticles + Glass Beads 28
3.2.4. X-Ray Diffraction 29
3.2.4.1. MG30, ethanol, and TiO_2 mixtures 29
3.2.4.2. MG80, ethanol, and TiO_2 mixtures 30
3.2.4.3. Heterogeneous Nucleation Method 32

Chapter 4 Structural Analysis

4.1. Sieve Analysis 34
4.1.1. Objectives 34
4.1.2. Methodology 34
4.1.3. Results 34
4.1.3.1. Particle Distribution 34
4.1.3.2. Fineness Modulus 36
4.1.3.3. Blends Fineness Modulus 36
4.1.3.4. Coefficient of uniformity 39
4.2. Scanning Electron Microscopy (SEM) 40
4.2.1. MG30 Recycled Glass 40
4.2.2. MG80 Recycled Glass 41
4.2.3. MG30 + TiO_2 Composites 42

4.2.4. MG80 + TiO_2 Composites 42
4.3. Surface Porosity 43
4.3.1. Objectives 43
4.3.2. Methodology 43
4.3.2.1. Sintering 43
4.3.2.1.1. Recycled Glass Powders 43
4.3.2.1.2. Recycled Glass Blends 43
4.3.2.1.3. Recycled Glass with TiO_2 particles 43
4.3.2.2. Polishing 44
4.3.2.3. Microstructure Analysis 44
4.3.3. Results 45
4.3.3.1. MG30 Recycled Glass 45
4.3.3.2. MG80 Recycled Glass 47
4.3.3.3. MG30 + MG80 Blends 50
4.3.3.4. MG30 and MG80 glasses sintered with TiO_2 particles 52
4.3.3.5. MG30 + MG80 blends sintered with TiO_2 particles 56
4.4. Percolation 58
4.4.1. Objectives 58
4.4.2. Methodology 58
4.4.2.1. Sintering 58
4.4.2.1.1. MG30 and Mg80 Recycled Glass Powders 58
4.4.2.1.2. MG30 and MG80 Recycled Glass Blends 58
4.4.2.1.3. MG30 and MG80 Recycled Glass Powders with TiO_2 particles 59
4.4.2.2. Analysis 59

4.4.3. Results & Discussion 61
4.4.3.1. Effects on MG30 and MG80 Recycled Glass 61
4.4.3.2. MG30 + MG80 Recycled Glass Blends 63
4.4.3.3. MG30 Recycled Glass Powder with TiO_2 particles 64
4.4.3.4. MG80- Recycled Glass Powder with TiO_2 particles 66

Chapter 5: Mechanical Analysis

5.1. Compression Test 68
5.1.1. Objectives 68
5.1.2. Specifications 68
5.1.3. Results 70
5.1.3.1. MG30 Recycled Glass 70
5.1.3.2. MG80 Recycled Glass 71
5.1.3.3. MG30 and MG80 Blends 72
5.1.3.4. MG30 with TiO_2 particles 73
5.1.3.5. MG80 with TiO_2 particles 75

Conclusions 77
References 79

List of Tables

Table 1: Release of contaminants to surface and groundwater. [13] 6

Table 2: XRD Data of titanium (IV) oxide anhydrous powder. 18

Table 3: TiO_2 optimum dosages for some organic pollutants degradation.[9] 22

Table 4: XRD data of MG30 with 1% titanium (IV) oxide anhydrous powder. 30

Table 5: XRD data of MG80 with 1% titanium (IV) oxide anhydrous powder. 31

Table 6: XRD data of MG30 with 1% titanium (IV) oxide anhydrous powder. 33

Table 7: Sieve Analysis 35

Table 8: MG-30 and MG-80 blends, fineness modulus (FM). 37

List of Figures

Figure 1: Schematic of SVE system.14 4

Figure 2: Air sparging system with SVE.[15] 8

Figure 3: Basic layout design of a PRB within a contamination plume.[16] 9

Figure 4: Glass generation and recovery from 1960 to 2010 in USA.[6] 11

Figure 5: Schematic of solid-state sintering mechanisms.[27] 13

Figure 6: Two-particle model made of glass spheres sintered at 1000°C for different times. [27] 14

Figure 7: Schematic of grain growth in porous pwders compacts. Arrows on the grain boundaries indicate the direction of boundary movement. 15

Figure 8: Schematic of the design criteria. 16

Figure 9: Diffraction patter of titanium (IV) oxide anhydrous powder. 19

Figure 10: Titanium (IV) oxide anhydrous particles at MG80 glass bead surface. 19

Figure 11: TGA/DTA analysis on Titanium (IV) Oxide Anhydrous powder with a heating rate of 5 °C/min in an air flow. 20

Figure 12: MG30 recycled glass sintered at 750ºC for 25 minutes (a) 0% TiO_2 at low magnification, (b) 1% TiO_2 at low magnification, (c) 1% TiO_2 at low magnification, and (d) 1% TiO_2 at high magnification. 26

Figure 13: MG80 recycled glass sintered at 725ºC for 25 minutes (a) 0% TiO_2 at low magnification, (b) 1% TiO_2 at low magnification, (c) 1% TiO_2 at low magnification, and (d) 1% TiO_2 at high magnification. 27

Figure 14: MG30 recycled glass, 6g/L PA pretreated and sintered at 800ºC for 20 minutes (a) 500 μm, (b)100 μm, (c)100 μm, and (d)10 μm. 28

Figure 15: Diffraction pattern of MG30 recycled glass sintered with 1% TiO_2. 29

Figure 16: Diffraction pattern of MG80 recycled glass sintered with 1% TiO_2. 31

Figure 17: Diffraction pattern of MG30 (0.30 mm) with a 3 g/L PA pretreatment with TiO_2 nanoparticles. 32

Figure 18: Passing percentage as a function of recycled glass particle size. 35

Figure 19: Blends fineness modulus as a function of MG30 percent. 38

Figure 20: SEM images of MG30 recycled glass sintered at 725ºC for 25 minutes, (a) magnification of 40X, (b) magnification of 100X. 40

Figure 21: SEM images of MG80 recycled glass sintered at 750ºC for 25 minutes, (a) 40X, (b) 100X. 41

Figure 22: SEM images of MG30 recycled glass beads mixed with 1% TiO_2 sintered at 800ºC for 20 minutes, (a) 500 μm, (b) 100 μm, (c) 20 μm. 42

Figure 23: SEM images of MG80 recycled glass beads mixed with 1% TiO_2 sintered at 800ºC for 20 minutes, (a) 500 μm, (b) 100 μm, (c) 20 μm. 42

Figure 24: Samples micrographs analysis using ImageJ. (a) Original micrograph, (b) processed image used in the ImageJ analysis. 45

Figure 25: Sintered glass micrographs of 1 gram of MG-30 recycled glass sintered for 15 minutes at (a) 700ºC, (b) 725ºC, (c) 750ºC, (d) 775ºC, and (e) 800ºC. 46

Figure 26: MG30 porosity as function of the sintering parameters. 47

Figure 27: Surface micrographs of 1 gram of MG-80 recycled glass sintered for 15 minutes at (a) 700ºC, (b) 725ºC, (c) 750ºC, (d) 775ºC, and (e) 800ºC. 48

Figure 28: MG-80 porosity as function of sintering parameters. 49

Figure 29: MG30-MG80 blend with (a) 85% MG30 recycled glass, (b) 10% MG30, (c) 100% MG30, and (d) 100% MG80, sintered at 750ºC for 30 minutes. 51

Figure 30: Porosity as a function of the amount of MG30 in each blend. 52

Figure 31: Optical micrographs of MG30 recycled glass with (a) 0.7% TiO_2, (b) 1% TiO_2, and (c) 0% TiO_2. All samples were sintered at 750ººC for 30 minutes. 54

Figure 32: Optical micrographs of MG30 recycled glass with (a) 0.7% TiO_2, (b) 1% TiO_2, and (c) 0% TiO_2. All samples were sintered at 750ºC for 30 minutes. 54

Figure 33: Recycled glass porosity changes according to TiO_2 percentage in MG30. .. 55

Figure 34: Recycled glass porosity changes according to TiO_2 percent present in MG80. 55

Figure 35: MG30-MG80 blends porosity changes by the addition of 1% TiO_2. Samples were sintered at 750ºC for 30 minutes. 57

Figure 36: Schematic of percolation apparatus. 60

Figure 37: Percolation apparatus. 60

Figure 38: Surface micrographs of: (a) MG-30, (b) MG-80 percolation samples sintered at 750ºC for 20 min. 61

Figure 39: MG-30 percolation as a function of sintering parameters. 62

Figure 40: MG-80 percolation as a function of sintering parameters. 62

Figure 41: Blends Percolation changes according to MG30 percentage. 63

Figure 42: Percolation of MG30 recycled glass sintered with TiO_2 particles at 800ºC for 20 minutes. 65

Figure 43: Percolation of MG80 recycled glass sintered with TiO_2 particles at 800ºC for 20 minutes. 67

Figure 44: MTS compression test machine. 69

Figure 45: MG30 compressive strength as function of the sintering parameters. 70

Figure 46: MG80 compressive strength as a function of sintering parameters. 71

Figure 47: Compressive strength of recycled glass blends as function of MG30 percentage for samples sintered at 750°C for 30 minutes. 73

Figure 48: MG30+TiO_2 composites compressive strength as function of TiO_2 percentage. 74

Figure 49: MG80+TiO_2 composites compressive strength as function of TiO_2 percentage. 76

List of Symbols

$A_{surface}$, specimen’s surface area

β, x-ray wavelength

Cu, coefficient of uniformity

D_{10}, grain diameter at 10%

D_{60}, grain diameter at 60%

FM, fineness modulus

F_{max}, fracture force

RA, retained accumulated percetage

τ, mean size of crystal

θ, Bragg angle

Δt, elapsed time of percolation V_w,water volume

List of Abbreviations

XRD, X-Ray Diffraction

SEM, Scanning Electron Microscope

TGA, Thermogravimetric Analysis

Chapter 1 Background

1.1. Introduction

Progress in science and technology, required to fulfill today's human lifestyle requirements are adversely affecting our natural resources. Global pollution, main cause of diseases such as asthma[1] and cholera[2], and of hunger and global warming, is the obvious product of the waste accumulation and industrialization that scathes air, water and soils with high agricultural value. Specifically, soil pollution results in a decrease in soil fertility and natural nutrients, as well as detrimental impact on the flora and fauna[2]. To deal with these problems new ideas and remediation methods are needed so as to sustain and regenerate our natural resources. One way to achieve this goal is by improving the implementation of recycled materials in sustainable products. Consequently, the main goal of the present work has been to construct a filter made of a recyclable material for the remediation or regeneration of polluted soils. The material selected for the proposed filter was recycled glass because this amorphous ceramic is one hundred percent recyclable with no loss of purity or quality[3]. To accomplish such goal, the present research is divided in three segments that focus on the filter structure, its mechanical characterization, and the subsequent pollutant degradation due to the designed system.

1.2. Soil Pollution

Soil pollution is caused by the alteration of natural soil with the presence of human-made chemicals. Soil pollutants encompass industrial wastes, pesticides, fertilizers, insecticides, as well as leakages from sanitary sewages and underground storage tanks[2]. All of these problems result from human malpractices such as engineering designs not compliant with environmental regulations, excessive usage of agricultural additives, and low supervision of soil related systems. All of them are harmful to our environment.

More regretfully, the whole ecosystem is affected by a polluted soil. Flora and agriculture are directly impacted by the indiscriminate use of fertilizers and pesticides. In particular fertilizers, which are commonly employed to correct soils deficiencies, can become harmful by contaminating the soil with impurities or derivatives from their decomposition or chemical reactivity. These products often contain ammonium nitrate (NH_4NO_3), phosphorus oxide (P_2O_5), and potassium oxide (K_2O) [4]. In addition to fertilizers, farmers use pesticides to prevent damaging plagues. Crops are constantly contaminated by pesticides remnants adsorbed by soil components. Human health is harmfully affected by the presence of the said pesticides in crops. Between 1961 and 1971, United States and South Vietnam armed forces used Herbicide Orange (also known as Agent Orange) to defoliate forests and to destroy 'unfriendly' crops as a tactic for decreasing enemy food supplies.[4] Agent Orange was later discovered to be contaminated with the dioxin TCDD, harmful pollutant that causes cancer, soft tissue sarcoma, type 2 diabetes, among other diseases.[4] Meanwhile, fauna is also affected by

this herbicide, with problems in the immune, endocrine, reproductive and nervous systems.[4] Contaminated crops and low quality products obtained by the misuse of agricultural agents are responsible for high industrial losses, and damage to food supplies and human health quality. Moreover, drinking water resources can also be affected by rain water percolation through polluted soils. Polluted water serves as another source for diseases like cholera brain damage. These facts strongly support the importance of the remediation of polluted soils.

Organic pollutants, such as fertilizers and pesticides, can be degraded by several methods such as soil washing, solvent extraction, and incineration[5]. Unfortunately, the majority of these processes are expensive.

In view of the aforementioned considerations, this thesis proposes the development of a low cost remediation system that consists of a sintered recycled glass filter to redress soils by percolation. In our system, pollutants can be degraded by a photo-catalytic reaction using titanium (IV) dioxide (TiO_2) as catalyst.

1.3. Soil Remediation Systems

1.3.1. Soil Vapor Extraction

Soil vapor extraction (SVE) is utilized to remove volatile organic compounds (VOCs) from soils in the unsaturated zone above the groundwater table. It consists of passing an air stream through the soil, thus transferring the contaminants from the soil matrix to the air stream.

These systems are implemented by installing vapor extraction wells in the affected zone and applying a vacuum to induce soil gases. SVE systems include knockout druses, followed by vapor-phase treatment prior to discharge to the atmosphere. Extraction wells effective radius varies from 6 m to 45 m, depending on soil conditions. The reported maximum depth of these SVE systems was 7 meters in soils with an average permeability of 10^{-4} cm/s. Figure 1 shows the SVE schematic design.

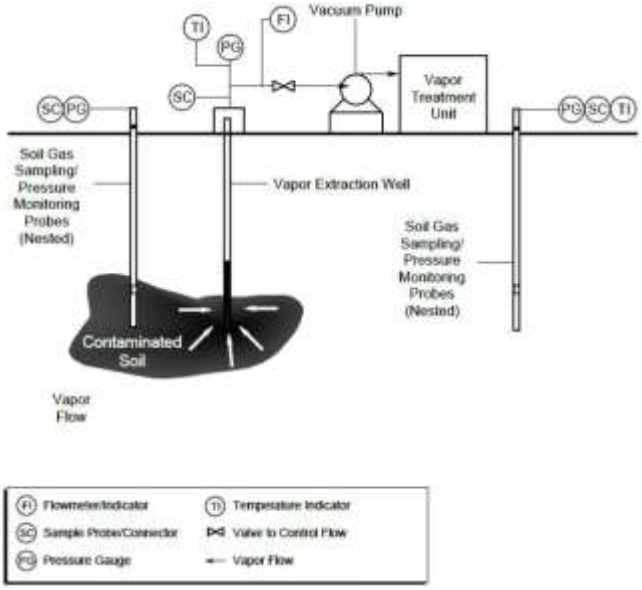

Figure 1: Schematic of SVE system.[14]

1.3.2. Soil Washing

Soil washing may be completed with water, aqueous extractive agents, solvents, or even air. The objective of this procedure is to separate the contaminated soil into two output streams: one clean and one contaminated. Washing can be done on the entire soil/sediment matrix or on selected portions. In one soil-washing project, 82% of the input sediment was completely cleaned.[16] Soil-washing process can effectively process large quantities of contaminated material.

In one example of the soil-washing process, first water is added to the soil and then the slurry is directed through a series of separating devices including a screened cylinder to separate materials coarser than 6 mm, cyclone separators to remove particles smaller than 45 μm, and a dense media separator to remove the less dense humic materials.

1.4. Ground Water Pollution

Every industrial and commercial facility generates wastewater. Ability to clean up wastewater is always less than 100%. Table 1 summarizes the source, volume release, and concentration of surface and groundwater pollutants.

Table 1: Release of contaminants to surface and groundwater. [13]

Source	Volume of release	Contaminant Concentration	Types of factors affecting release
Transport Spills	Partial to entire contents of Transport vessel	High	Traffic accidents; unloading mishaps
Storage Spills	Partial to entire content of storage vessels	High	Structural failure of tank; mishaps in handling
Leaks	Minimal Rate; yet could continue indefinitely, particularly if underground	High	Frequency of inspections and maintenance; age of storage facilities
Treatment Effluent	Varies often high	Low (required by regulatory permits)	Influent; design and operation of facility
Landfills Runoff	Possibly large, depending on rainfall event	Low; typically contaminated sediment; nil if landfill is capped	Integrity of cap; slope; storm water retention
Surface seeps	Minimal rate; yet could continue indefinitely	Medium to high	Characteristics of cap (slope and permeability); disposal of liquids; removal of leachate
Leachate through base	Minimal to low rate for lined facilities; moderate to high rate for unlined facilities; continues indefinitely	Medium to high	Same as above plus permeability of base.
Lagoons Overflow, washout	Partial to entire contents	High (stored hazardous waste)	Structural failure; flooding
Leakage	Minimal to low rate for lined facilities, moderate to high for unlined facilities; continues indefinitely	High (stored hazardous waste)	Permeability of base; liquid depth

1.5. Ground Water Remediation Systems

Ground water remediation systems are selected according to contaminant and soil properties, the most important ones being its chemical composition and diffusion properties. Moreover, soil properties, such as grain size distribution and percolation, play a major role in the selection of the most effective remediation system.

The first step for ground water remediation is to inhibit the contaminant flow to clean groundwater. Vertical barriers prevent the migration of contaminants and can be classified in up-gradient or down-gradient ones. Up-gradient vertical barrier walls provide a cutoff controlling the influx of clean groundwater flow from up-gradient regions. When used with a pumping system located on the down-gradient side, groundwater withdrawal may contain contaminants that have migrated down-gradient of the site. Moreover, down-gradient cutoff walls are effective in aiding the pump-and-treat system to speed removal of contaminants from the subsurface.

1.5.1. Pump and Treat Remediation System

The main objective is to remove chemical mass from the ground water. After removing the contaminated water one applies water treatment methods such as air stripping, carbon absorption methods, and biological treatment for organics. Some limitations of this process are that chemical concentrations detected in groundwater extraction wells typically have shown a fast initial decrease of groundwater extraction followed by a decreasing rate of chemical removal[18].

1.5.2. Air Sparging

Air sparging (Figure 2), used for the remediation of groundwater contaminated with volatile organics, involves the air injection into the subsurface (in the saturation zone) to force transfer of volatile organic contaminants from the aqueous phase onto the vapor phase.19 This process is normally conducted in conjunction with soil vapor extraction implemented in the unsaturated zone. The principal benefits of air sparging are the in situ volatilization of dissolved-phase contaminants, the desorption and vitalization of contaminants adsorbed to the soil matrix, and the enhanced aerobic biodegradation. Some limitations of this process is that the transfer of contaminants are from one medium (water) to another (air), thus increasing the amount of contaminants in the atmosphere.

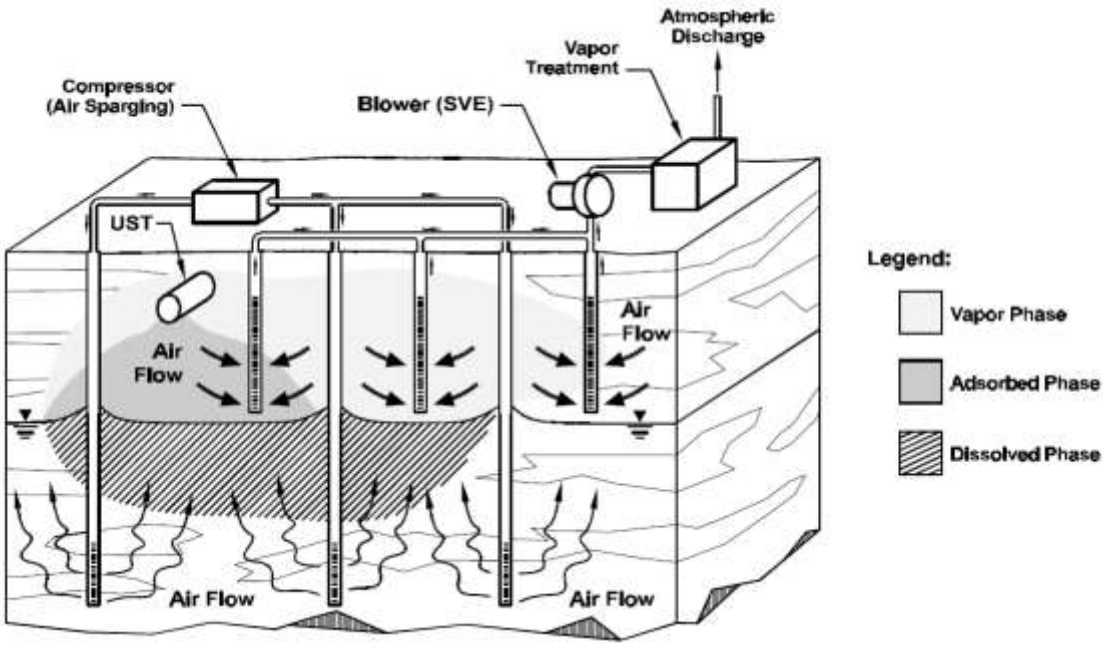

Figure 2: Air sparging system with SVE.[15]

1.5.3. Permeable Reactive Barriers

Permeable reactive barriers (PRB) are installed across the flow path of a contaminant plume to remove contaminants present in the groundwater. Contaminants are removed by physical, chemical, and/or biological processes that include fixation, degradation, oxidation/reduction, sorption, and precipitation[17]. These systems contain the chemical mass present in groundwater while allowing uncontaminated groundwater flow to pass through the wall. The major advantage of PRBs is that they do not require a continuous input of energy to run pumps or treatment systems[17]. This reduces operation and maintenance costs. Figure 3 shows a basic layout of a permeable treatment barrier.

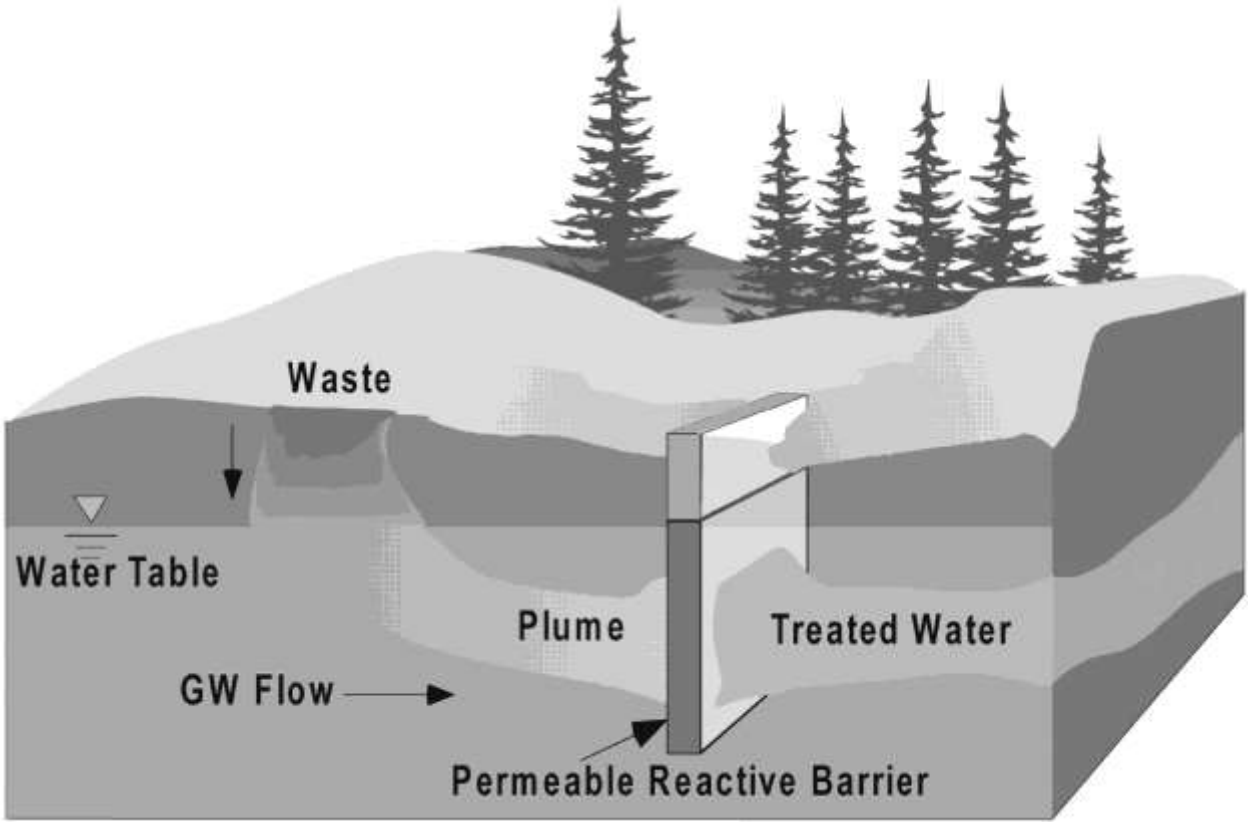

Figure 3: Basic layout design of a PRB within a contamination plume.[16]

1.5.4. Degradation Treatment Walls

Degradation treatment walls (DTW) are designed to degrade contaminants in groundwater by employing either enhanced biological degradation or chemical destruction mechanisms. Zero valence metallic iron (Fe0) is generally used to create reducing conditions that destroy chlorinated solvents such as tethrachloroethylene (TCE) and perchloroethylene (PCE).20

In DTW aerobic groundwater enters the iron filling wall, and causes the oxidation of metallic iron (Fe0) to ferrous iron (Fe2+) with the subsequence release of two electrons (Equation 1). Chlorinated solvents such as PCE will react as electron acceptors, resulting in dechlorination and release of a chloride ion (Equation 2).

$$\mathbf{Fe^0 \rightarrow Fe^{2+} + 2e^-} \qquad \text{Equation 1}$$

$$\mathbf{RCl + 2e^- + H^+ \rightarrow RH + Cl^-} \qquad \text{Equation 2}$$

1.6. Glass Recycling

According to the United States Environmental Protection Agency (EPA), glass employs 4.6% from total waste generation.[6] However, in 2010 only 27.1% of generated glass was recovered according to Figure 4. Such low percentage demonstrates the importance of generating new applications and uses for recycled glass.

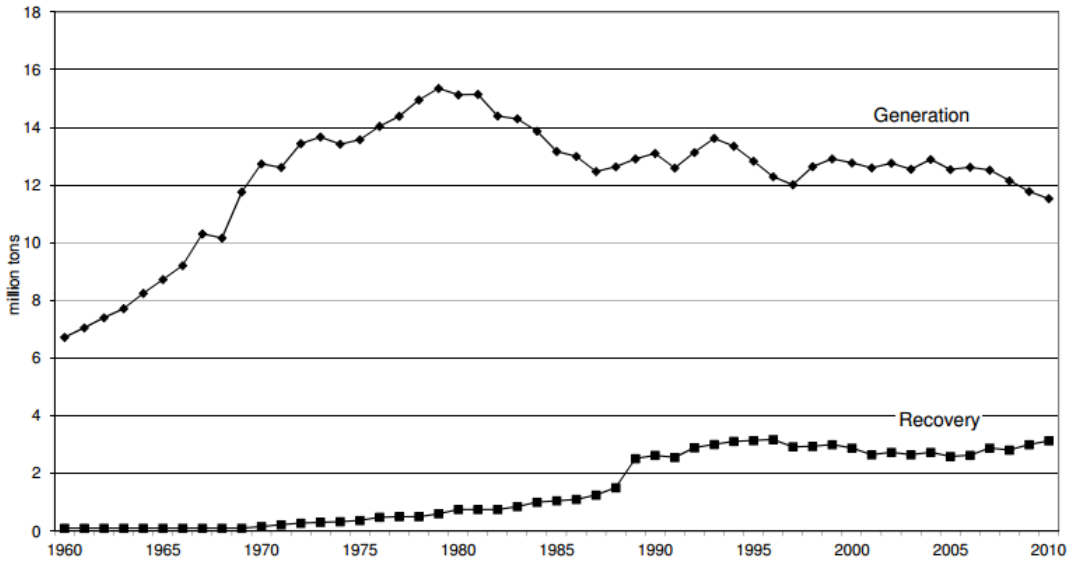

Figure 4: Glass generation and recovery from 1960 to 2010 in USA.[6]

Glass recycling is critical because of the chemical stability of this material: A glass bottle can take up to a million years to break down in a landfill.[3] Furthermore, glass recycling is an unsophisticated process[3]. New glass containers can appear in a store in just a month after its recovery. Almost all glass containers are 100% recyclable, which means they can be recycled repeatedly, with no excessive loss of purity or quality.[3]

Since global warming is one consequence of industrialization, garbage generation, and carbon dioxide emissions, glass recycling treats this problem by reducing energy consumption, garbage and carbon dioxide emissions. Typically, the production of glass containers requires high amounts of energy due the high sintering times and temperatures needed. Yet, recycled glass products consume 40% less energy than the ones obtained directly from raw materials. Additionally, a ton of recycled glass saves

1,300 pounds of sand, 410 pounds of soda ash, and 380 pounds of limestone[3]. As one can see, glass recycling is the foundation for an unlimited number of benefits

1.7. Sintering

Sintering is referred to the heat treatment process applied to powders or porous materials in order to obtain a useful solid. This process is achieved by heating the powder compact or porous material to a temperature of 50% to 80% of its melting temperature.[26]

In the sintering processes we have variables such as temperature, gas atmosphere, solutes concentration, and defect chemistry. Fick's diffusion laws are used to predict how sintering processes rate are affected by these variables. Within this approach, matter is analyzed in terms of the concentration gradient of diffusion species expressed in terms of the chemical potential. Matter transport occurs from regions of higher chemical potential to regions of lower chemical potential. [26]

1.7.1. Solid-state sintering

Six mechanisms of sintering occur in solid state sintering: surface diffusion, surface lattice diffusion, vapor transport, grain boundary diffusion, grain boundary lattice diffusion, and plastic flow.[27] Figure 5 shows the six sintering mechanism present in solid-state sintering.

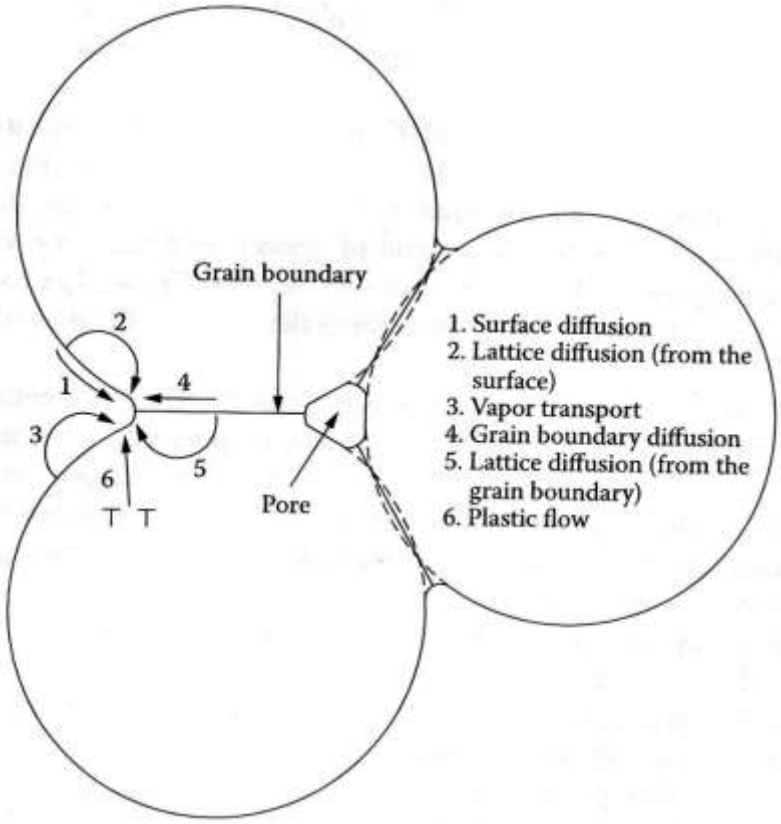

Figure 5: Schematic of solid-state sintering mechanisms.[27]

All the mentioned mechanisms lead to bonding and growth of necks between particles, so the strength of the powder compact increases during sintering. Sintering mechanisms can be divided as *densifying* and *nondensifying* mechanisms.[27] *Densifying* mechanisms, such as grain boundary diffusion and lattice grain boundary diffusion, lead to shrinkage or densification of materials. Meanwhile, *nondensifying* mechanisms, such as surface diffusion, lattice diffusion, and vapor transport lead to neck growth without densification. [27]

1.7.2. Viscous Sintering

In amorphous materials, such as glass, matter transport occurs predominantly by viscous flow, this process is known as viscous sintering. In this type of materials, we don't have grain boundaries, thus neck growth and densification occur by viscous flow that involves the deformation of the particles. Figure 6 shows a two-particle model of glass spheres sintered at 1000°C for different times. We can clearly see the neck growth as sintering time increases. [27]

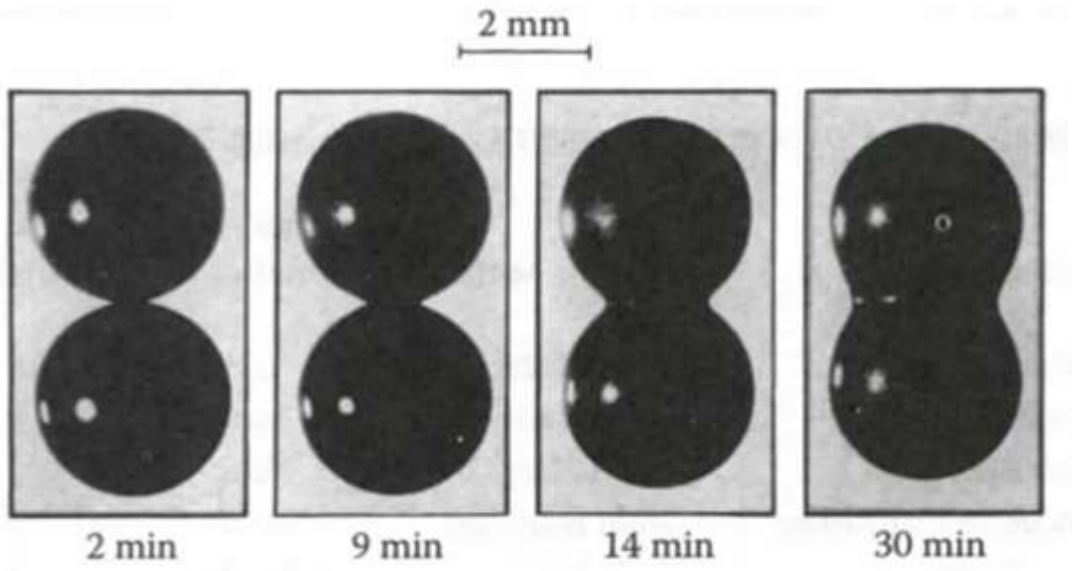

Figure 6: Two-particle model made of glass spheres sintered at 1000°C for different times. [27]

1.7.3. Grain Growth in Porous Media

Greskovich and Lay suggested a model for grain growth in porous materials. The model is shown in Figure 7. They assumed that surface diffusion assisted in the rounding on the particles and the growth of the necks between the particles. Whether the boundary can migrate depends on whether the structure permits it, i.e. there must be a decrease in the total energy of the system for an incremental movement of the boundary. [28]

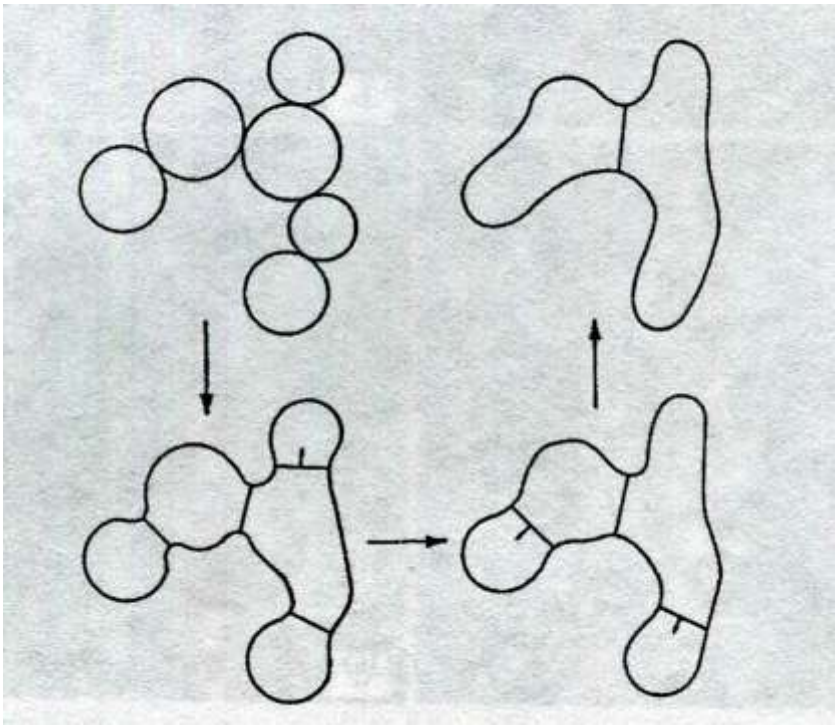

Figure 7: Schematic of grain growth in porous pwders compacts. Arrows on the grain boundaries indicate the direction of boundary movement.

Chapter 2 Problem Statement

2.1 Main Idea

The central purpose of this thesis has been to design, fabricate and characterize filters made of sintered recycled glass and TiO_2 particles for the degradation of organic pollutants.

2.2 Design Criteria

The remediation design, schematically shown in Figure 8, consists of a sintered recycled glass filter located under a layer of polluted soil. Rain water percolation across the soil carries soil pollutants towards and through the recycled glass filter. After this, soil pollutants are degraded at the filter by a photo-catalytic reaction produced by titanium dioxide particles.

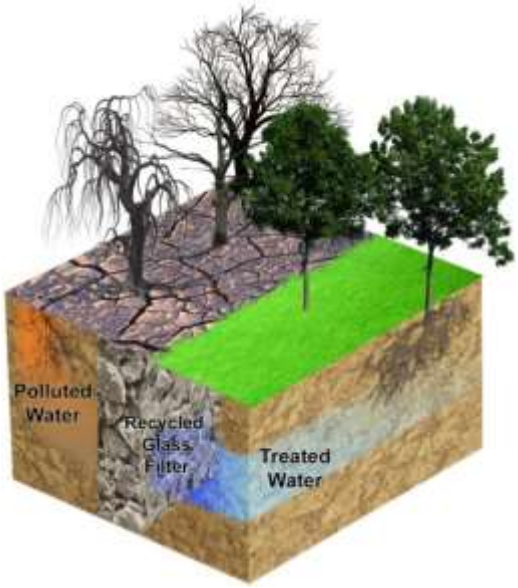

Figure 8: Schematic of the design criteria.

2.3 Materials Specifications

2.3.1. Recycled Glass Powder

The filter was fabricated by sintering two recycled glass powders provided by Vitro Minerals: MG-30 and MG-80[7]. MG recycled glass powders are white colored and obtained from plate glass[7]. Particle size ranges from 0.230 to 0.600 mm for the MG-30 and from 0.017 to 0.180 mm for the MG-80.[7]

2.3.2. TiO_2 Particles

Two methods were used for the functionalization of recycled glass beads surface for the degradation of soil pollutants. The first one consisted of titanium (IV) oxide anhydrous powder (TiO_2), ethanol and the recycled glass powder. The second one was by forming the dioxide via heterogeneous nucleation method on the glass beads. X-ray diffraction (XRD) was used to determine the polymorph structure of the TiO_2 phase, i.e. rutile or anatase, and the particle size. Moreover, TiO_2 particles surface morphology was observed by scanning electron microscopy (SEM). Finally, a thermo-gravimetric analysis (TGA) was performed to TiO_2 particles to characterize the particles thermal stability.

2.3.3. X-Ray Diffraction

Figure 9 shows the diffraction pattern of titanium (IV) oxide anhydrous powder. The 2θ peaks at 25.325° and 48.05° confirm TiO_2 anatase polymorph. The average particle size was calculated according to Scherrer's formula (Equation 3)[21]. Titanium (IV) oxide anhydrous powder presented an average particle size is of 12.17 nm. Table 2 summarizes the calculated data from Figure 9. Figure 10 shows a SEM micrograph of Titanium (IV) oxide anhydrous particles.

$$\tau = \frac{0.9\lambda}{\beta \cos\theta} \qquad \text{Equation 3}$$

where:

τ, mean size of crystal (nm)

λ , x-ray wavelength (nm)

β, width at half the maximum intensity, denoted FWHM (radians)

θ, Bragg angle (radians)

Table 2: XRD Data of titanium (IV) oxide anhydrous powder.

2θ (°)	d (Å)	Height	Area	FWHM	Crystallite Size (nm)
3.06	3.85	4138.80	37097.50	0.675	12.03
25.30	3.52	49358.50	392100.80	0.675	12.08
37.80	2.38	7437.80	66370.20	0.675	12.46
48.06	1.89	11024.30	110009.80	0.750	11.62
53.92	1.70	6813.50	67883.80	0.750	11.90
55.10	1.67	6676.00	66734.30	0.750	11.97
62.73	1.48	5158.20	51412.70	0.750	12.43
68.81	1.36	2311.70	23043.70	0.750	12.86
Average					**12.17**
Standard Deviation					**0.391**
Standard Error					**0.175**

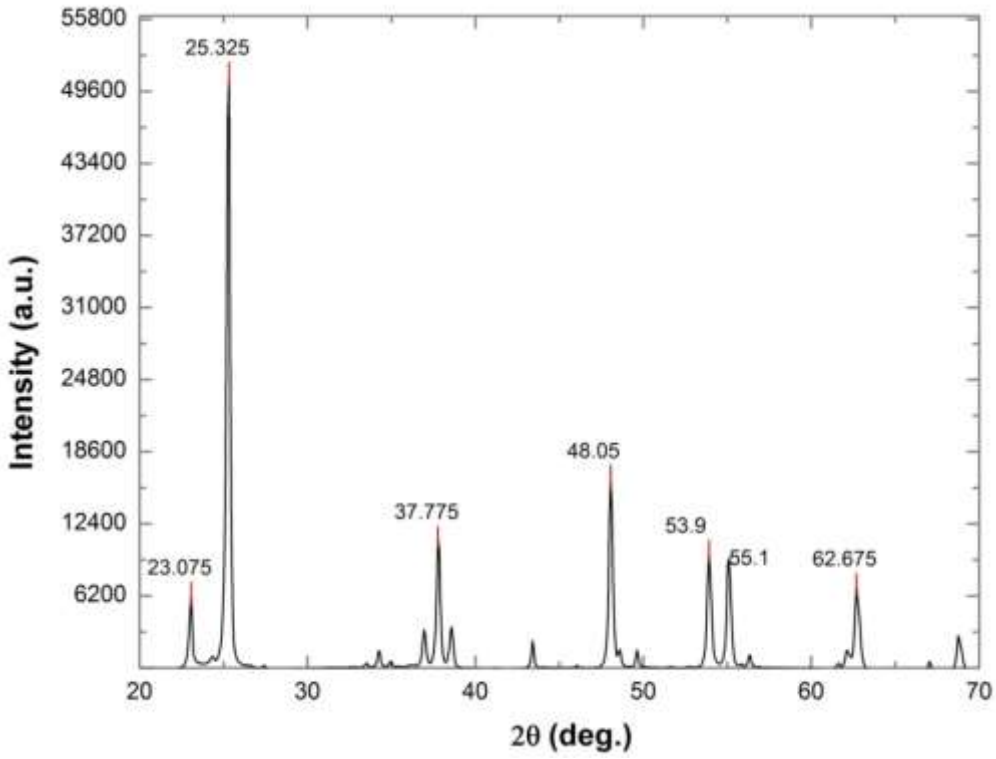

Figure 9: Diffraction patter of titanium (IV) oxide anhydrous powder.

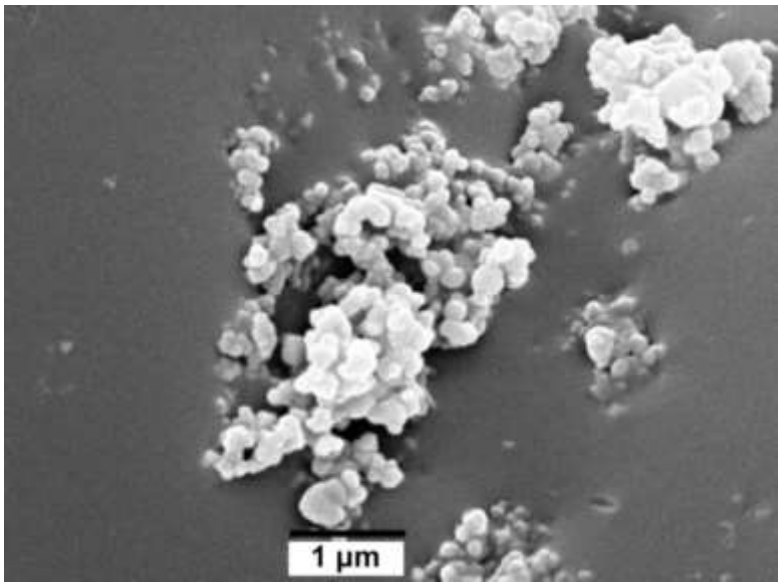

Figure 10: Titanium (IV) oxide anhydrous particles at MG80 glass bead surface.

2.3.4. Thermogravimetric Analysis (TGA)

A thermogravimetric analysis was performed to titanium (IV) oxide anhydrous powder. The test was conducted in air with a heating rate of 5°C/min. We can observe at the TGA curve shown in Figure 11 an initial weight decrease of 0.2% weight due evaporation of water at 100°C. Then we observe single stage decomposition from 105°C to 900°C of 5.24% weight. The DTA shows the endothermic reaction due evaporation of water molecules.

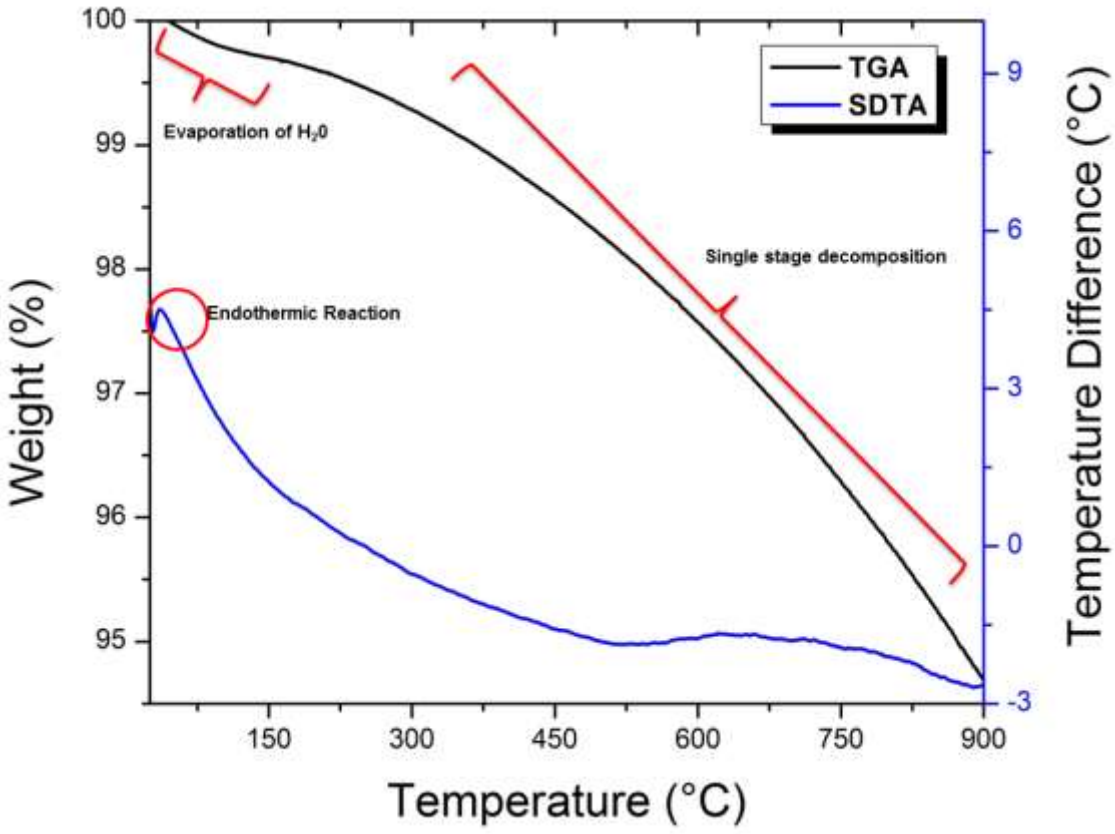

Figure 11: TGA/DTA analysis on Titanium (IV) Oxide Anhydrous powder with a heating rate of 5 °C/min in an air flow.

Chapter 3: Pollutant Degradation

3.1. Photocatalytic Activity

3.1.1. Introduction

Organic pollutants can be degraded by a photocatalytic reaction achieved by irradiating semiconductors such as TiO_2, ZnO, and Fe_2O_3. The photo-corrosion resistance and wide band gap energies make these metal oxide semiconductors one of the most suitable photocatalysts[22]. Table 2 presents the band gap energies and corresponding wavelength for several semiconductors.

Table 2: Band gap energies of several semiconductors at a certain wavelenght.

Semiconductor	Band gap energy (eV)	Wavelength (nm)
TiO_2 (rutile)	3.0	413
TiO_2 (anatase)	3.2	388
ZnO	3.2	388
ZnS	3.6	335
CdS	2.4	516
Fe_2O_3	2.3	539

TiO_2 has been widely used in water and waste water treatments studies because it is thermally stable, non-toxic, chemically and biologically inert and is capable of promoting oxidation of organic compounds[24]. The photocatalytic activity of TiO_2 depends on the composition, surface area, particle size distribution, porosity and band gap energy [25]. Table 3 summarizes the optimum dosage of TiO_2 for the degradation of several organic pollutants.

Table 3: TiO_2 optimum dosages for some organic pollutants degradation.[9]

Target compound	Usage	Photocatalyst	Optimum dosage (g/L)
Erioglaucine	Herbicide	TiO_2	0.30
Tebuthiuron	Herbicide	TiO_2	5.00
Propham	Herbicide	TiO_2	5.00
Triclopyr	Herbicide	TiO_2	2.00
Phorate	Insecticide	TiO_2	0.50
Trichlorfon	Insectiside	TiO_2	8.00
Carbendazim	Fungicide	TiO_2	0.07
Carbofuran	Insecticide	TiO_2	0.10
Glyphosate	Herbicide	TiO_2	6.00
Picloram	Herbicide	TiO_2	2.00
Fluometuron	Herbicide	TiO_2	3.00
Imazapyr	Herbicide	TiO_2	2.50

3.1.2. Fundamentals of photocatalytic reactions

Electron and hole pairs are generated when wide band gap semiconductors such as TiO_2 are irradiated with energy higher than their band gap energy (Equation 4). In this process the electrons are promoted to the conductive band (e_{CB}^-) leaving a positive hole in the valence band (h_{VB}^+). [9]

$$\mathbf{TiO_2 + hv\ (< 387\ nm) \rightarrow e_{CB}^- + h_{VB}^+} \qquad \text{Equation 4}$$

In Equation 6, h_{VB}^+ and e_{CB}^- are powerful oxidizing and reducing agents that react with organic compounds (R) such as pesticides, resulting in their oxidation producing CO_2 and H_2O as end products (Equation 5). [9]

$$\mathbf{h_{VB}^+ + R \rightarrow intermediates \rightarrow CO_2 + H_2O} \qquad \text{Equation 5}$$

The h_{VB}^+ species can also oxidize organic compounds by reacting with water to generate $OH^{\cdot}$ hydoxyl radical which has the second highest oxidation potential of 2.80 V (Equation 6).[9]

$$\mathbf{H_2O + h_{VB}^+ \rightarrow OH^{\cdot} + H^+} \qquad \text{Equation 6}$$

$OH^{\cdot}$ oxidizes almost all electron-rich organic molecules converting them to carbon dioxide and water (Equation 7).[9]

$$\mathbf{OH^{\cdot} + R \rightarrow intermediates \rightarrow CO_2 + H_2O} \qquad \text{Equation 7}$$

3.2. Recycled Glass Powder Surface Functionalization

3.2.1. Objectives

- Fabricate recycled glass beads + TiO_2 composites for the degradation of soil pollutants.
- Obtain the best method to attach the TiO_2 particles uniformly on the recycled glass beads surface.
- Determine the most economically viable method for the fabrication of recycled glass beads and TiO_2 composites.
- Determine the TiO_2 particle size obtained by the two studied methods.

3.2.2. Methodology

3.2.2.1. Recycled glass and titanium (IV) oxide anhydrous powder

For mixtures, we poured 10 mL of C_2H_60 and 20 mL of H_20 at 30 grams of recycled glass beads and 0.30 grams of titanium (IV) oxide anhydrous powder. The glass beads with TiO_2 were sintered and analyzed using SEM and XRD.

3.2.2.2. Heterogeneous Nucleation Method

To achieve a stronger interface between TiO_2 nanoparticles and glass beads, rough glass surface was necessary. A pretreatment of the glass beads of Pythic acid (PA) allowed etching the glass beads surface and causing that roughness. After the pretreatment, the TiO_2 particles could form more readily on the recycled glass surface via heterogeneous nucleation.

3.2.2.2.1. Recycled Glass Pretreatment

Recycled glass beads with an average particle size of 0.300 mm were pretreated with different concentrations of pythic acid solution of 0, 3, 6 g/mL. Hereon the treated glass is named as MGX0 /PA3, MG30/PA6, respectively where X=3 for MG30 and X=8 for MG80.

3.2.2.2.2. Synthesis of TiO_2 Nanoparticles + Glass Beads

Two solutions were prepared for the synthesis:

Solution 1: 10 grams of pretreated recycled glass beads, 0.1 g of tin (IV) chloride pentahydrate and 20 ml of ethanol.

Solution 2: 3.6 ml of tetrabutyl titanate, 0.4 ml acetyl acetone, 20 ml ethanol, and 6.0 ml H_2O were added to the second solution with vigorous stirring. A limpid yellow solution was formed by drop wise addition of hydrochloric acid (HCl) into the precipitate. Then **Solution 2** was poured into **Solution 1** and refluxed at 80ºC for 50 min. The as-prepared samples were cleaned carefully with anhydrous ethanol and de-ionized water.

3.2.3. Results

3.2.3.1. Scanning Electron Microscope (SEM)

3.2.3.1.1. MG30, ethanol, and TiO_2 mixtures

Figure 12 shows micrographs of MG30 recycled glass sintered at 750ºC for 25 minutes. The mixtures consisted of 0.30 g of titanium (IV) oxide anhydrous powder mixed with 30 g of MG30 recycled glass. Figures 12b, 12c and 12d reveal the formation of TiO_2 particles on the glass bead surface. Although most of those recycled glass beads were covered with TiO_2, the distribution was not uniform.

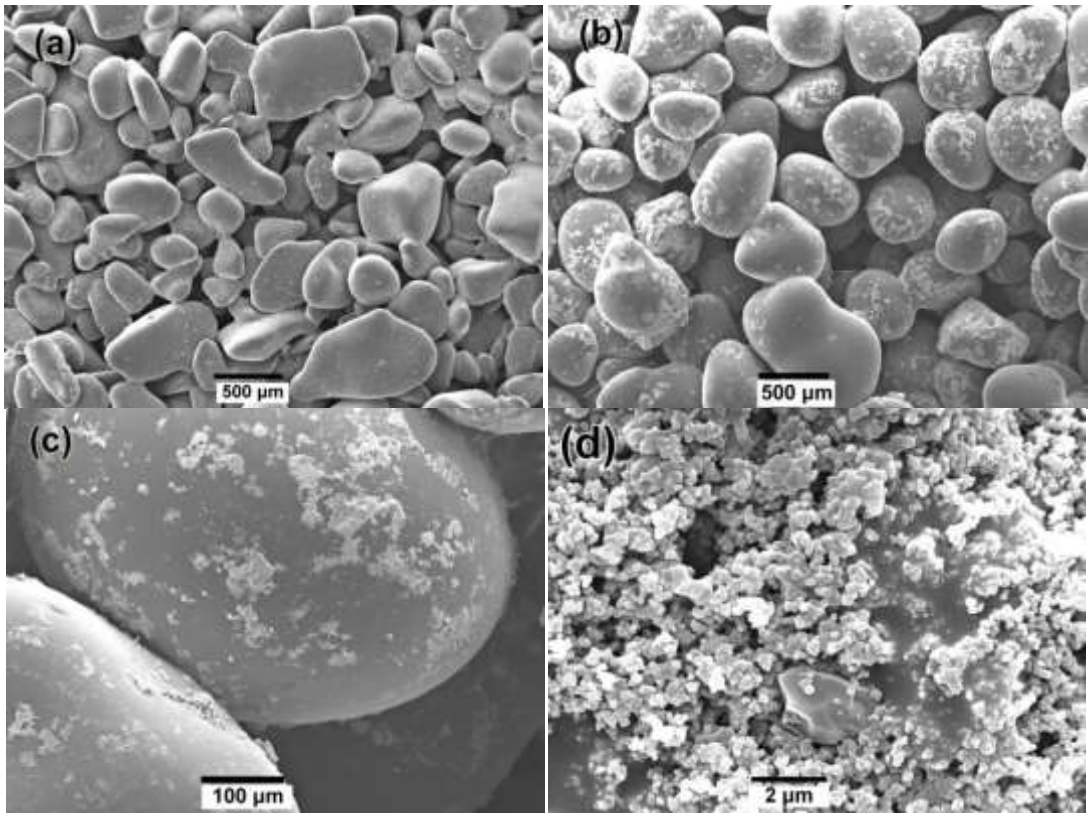

Figure 12: MG30 recycled glass sintered at 750ºC for 25 minutes (a) 0% TiO_2 at low magnification, (b) 1% TiO_2 at low magnification, (c) 1% TiO_2 at low magnification, and (d) 1% TiO_2 at high magnification.

3.2.3.1.2. MG80, ethanol, and TiO_2 mixtures

Figure 13 shows micrographs of MG80 recycled glass sintered at 725ºC for 25 minutes. Once again the mixtures consisted of 0.30 g of TiO_2 powder mixed with 30 g of MG80 recycled glass. Figure 13b shows how the addition of TiO_2 particles increased the sample void size by changing shape of MG80 particles. Figures 13c and 13d show the formation of TiO_2 particles on the surface of the MG80 beads. The distribution of TiO_2 was not uniform.

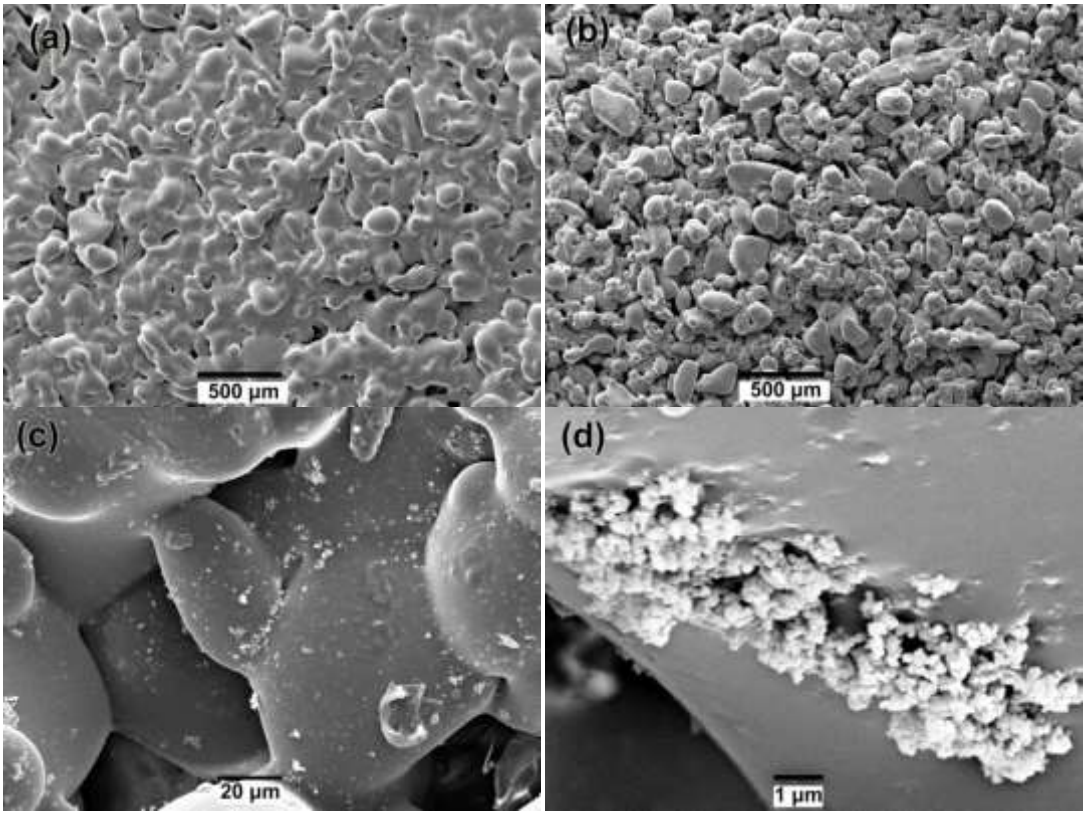

Figure 13: MG80 recycled glass sintered at 725ºC for 25 minutes (a) 0% TiO_2 at low magnification, (b) 1% TiO_2 at low magnification, (c) 1% TiO_2 at low magnification, and (d) 1% TiO_2 at high magnification.

3.2.3.1.3. Synthesis of TiO_2 Nanoparticles + Glass Beads

Figure 14 shows SEM micrographs of MG30 recycled glass beads pretreated with 6g/L PA. The sample was sintered at 800°C for 20 minutes. In Figure 14b the increase in beads roughness after the PA pretreatment is apparent. Such roughness improved the nucleation and distribution of TiO_2 particles across recycled glass beads surface as shown in Figure 14c. Figure 14d shows the morphology of some agglomerated particles of the synthesized TiO_2 particles.

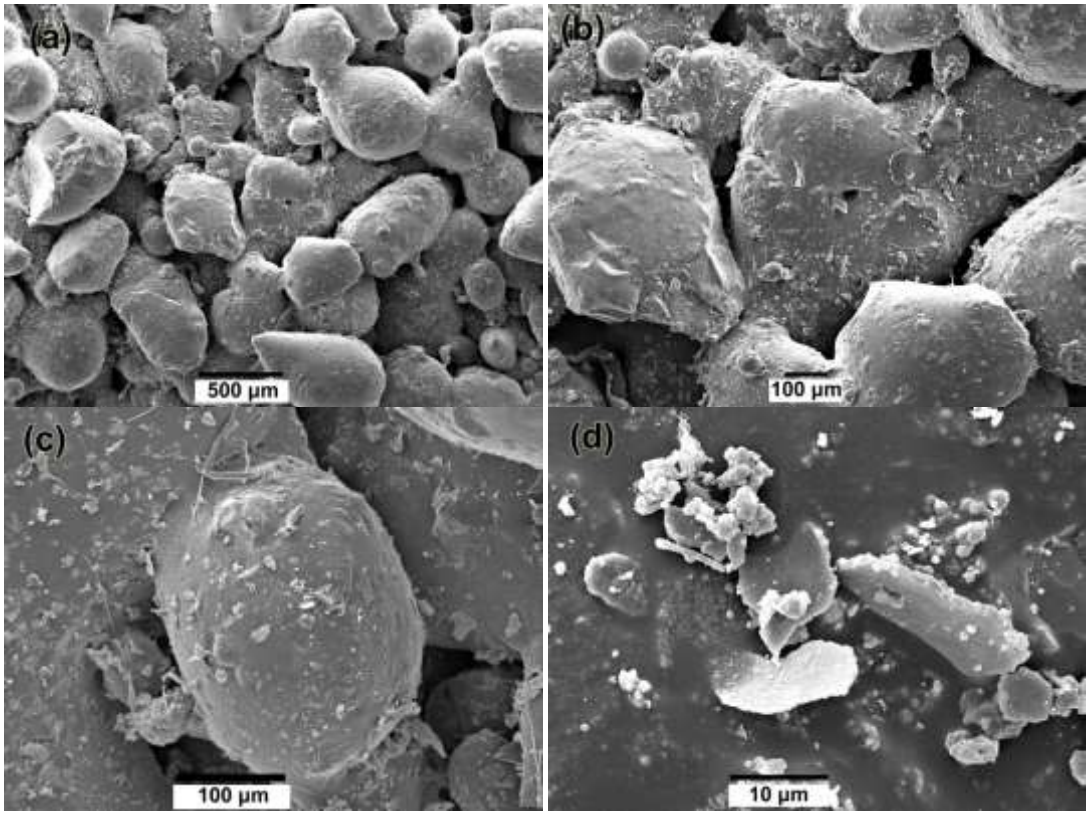

Figure 14: MG30 recycled glass, 6g/L PA pretreated and sintered at 800ºC for 20 minutes (a) 500 µm, (b)100 µm, (c)100 µm, and (d)10 µm.

3.2.4. X-Ray Diffraction

3.2.4.1. MG30, ethanol, and TiO_2 mixtures

Figure 15 shows the diffraction pattern of MG30 recycled glass sintered with 1% TiO_2. The shown peaks are characteristics of the anatase polymorph of TiO_2. Using the Scherrer's expression (Equation 3) we calculated an average particle size of 11.79 nm for TiO_2 particles. Table 4 summarizes the calculated data from Figure 15.

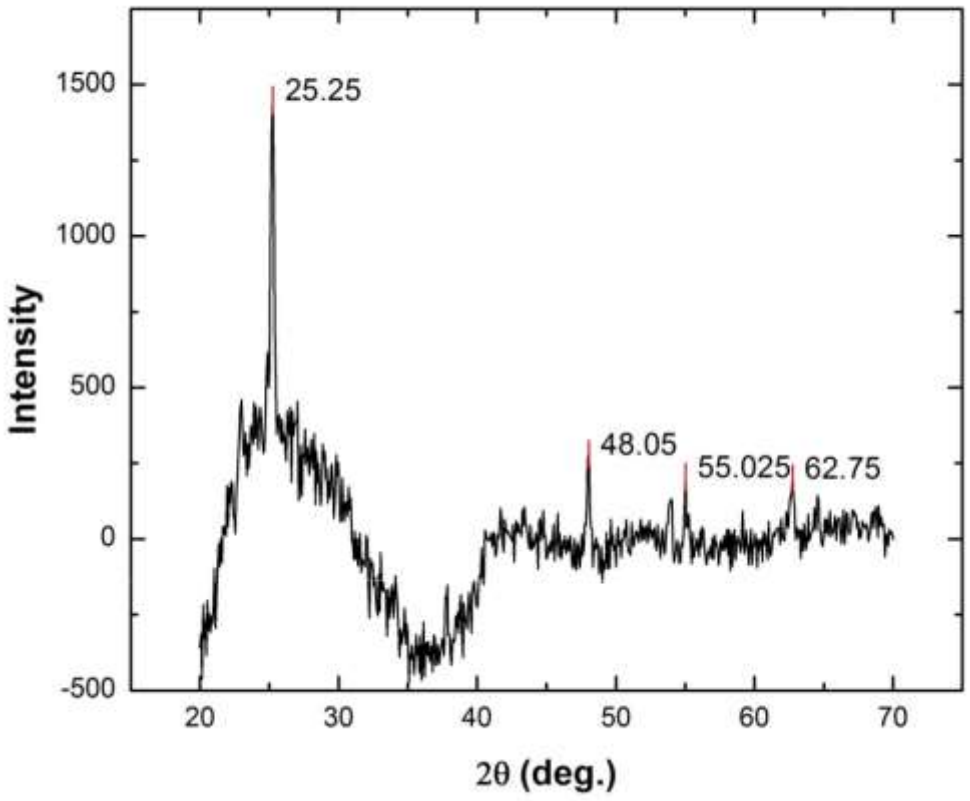

Figure 15: Diffraction pattern of MG30 recycled glass sintered with 1% TiO_2.

Table 4: XRD data of MG30 with 1% titanium (IV) oxide anhydrous powder.

2θ (°)	d (Å)	Height	Area	FWHM	Crystallite Size (nm)
23.00	3.86	4492.9	40435.7	0.675	**12.03**
25.23	3.53	5247.6	56505.5	0.825	**9.88**
37.65	2.386	2100.3	18837.4	0.675	**12.46**
47.98	1.89	1799.1	19788.5	0.825	**10.56**
53.89	1.70	1651.2	14860.5	0.675	**13.22**
55.09	1.67	1668.6	16685.3	0.750	**11.97**
62.66	1.48	1625.2	16250.6	0.750	**12.42**
Average					**11.79**
Standard Deviation					**1.16**
Standard Error					**0.44**

3.2.4.2. MG80, ethanol, and TiO_2 mixtures

The diffraction pattern of MG80 recycled glass sintered with 1% TiO_2 is shown in Figure 16. The shown peaks are characteristics of the anatase polymorph of TiO_2. Using the Scherrer's expression (Equation 3) we calculated an average particle size of 34.40 nm for TiO_2 particles. We can observe a difference of almost 66% between MG30 and MG80 TiO_2 crystallite size. This behavior is due the available surface area that TiO_2 particles have for attachment. MG80 beads are smaller than MG30's, thus TiO_2 particles will be more agglomerated. Moreover the difference among TiO_2 and MG30 beads is high so TiO_2 particles cannot agglomerate in the same way they do at the MG80. Table 5 summarizes the calculated data from Figure 16.

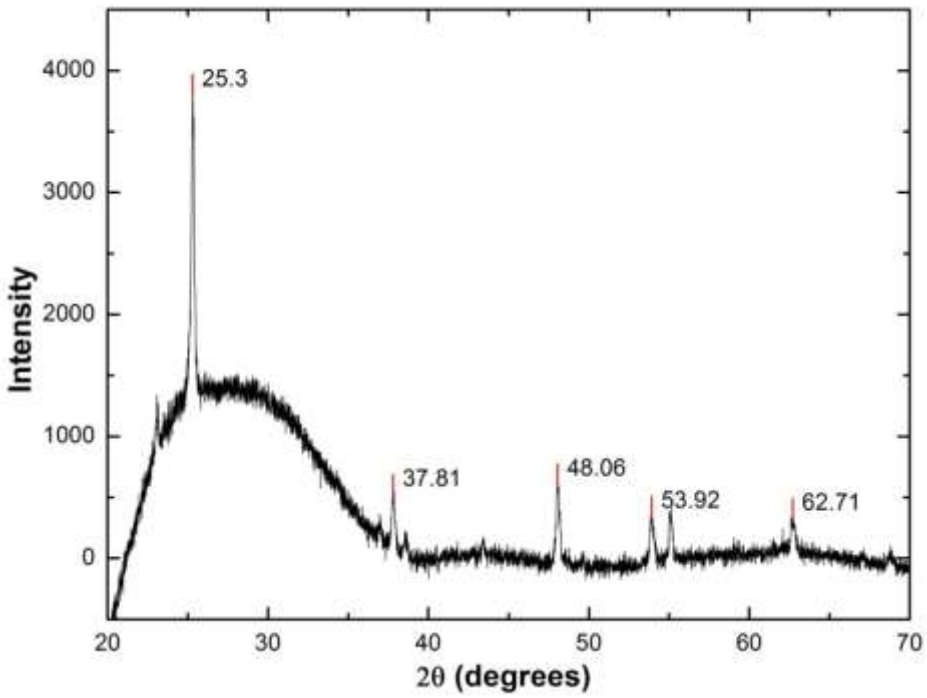

Figure 16: Diffraction pattern of MG80 recycled glass sintered with 1% TiO_2.

Table 5: XRD data of MG80 with 1% titanium (IV) oxide anhydrous powder.

2θ (°)	d (Å)	Height	Area	FWHM	Crystallite Size (nm)
25.31	3.52	2519.83	31319.70	0.20	40.78
37.81	2.38	458.20	12556.93	0.25	33.64
48.06	1.89	645.17	18177.13	0.26	33.51
53.91	1.70	403.93	12293.50	0.29	30.78
62.71	1.48	307.75	9329.65	0.28	33.28
25.31	3.52	2519.83	31319.70	0.20	40.78
37.81	2.38	458.20	12556.93	0.25	33.64
Average					**34.40**
Standard Deviation					**3.76**
Standard Error					**1.68**

3.2.4.3. Heterogeneous Nucleation Method

The heterogeneous nucleation method was successful for the synthesis of TiO_2 nanoparticles on the recycled glass beads surface. Figure 17 shows the diffraction pattern of MG30 glass beads with TiO_2 nanoparticles. Each peak shown in Figure 17 is characteristic of the TiO_2 rutile polymorph. Using equation 3 we calculated the TiO_2 crystallite size for each descriptive peak. The average particle size of TiO_2 nanoparticles was of 9.82 nm. Table 6 summarizes the calculated data from Figure 17.

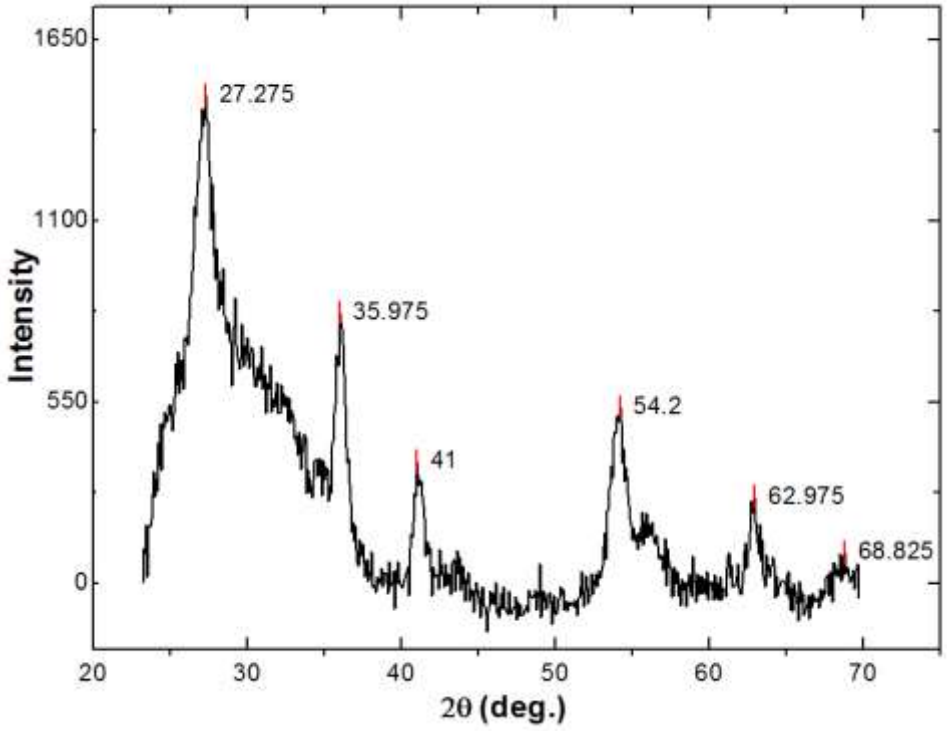

Figure 17: Diffraction pattern of MG30 (0.30 mm) with a 3 g/L PA pretreatment with TiO_2 nanoparticles.

Table 6: XRD data of MG30 with 1% titanium (IV) oxide anhydrous powder.

2θ (°)	d (Å)	Height	Area	FWHM	Crystallite Size (nm)
27.20	3.28	519.95	8327.15	1.11	7.38
36.06	2.49	506.00	5560.90	0.73	11.40
41.05	2.20	277.80	3602.60	0.90	9.45
54.11	1.70	353.30	5262.50	1.00	8.91
62.87	1.48	197.47	2165.73	0.78	11.96
Average					**9.82**
Standard Deviation					**1.87**
Standard Error					**0.84**

Chapter 4 Structural Analysis

4.1. Sieve Analysis

4.1.1. Objectives

- Corroborate MG30 and MG80 recycled glass powders particle size distribution.
- Obtain MG-30 and MG-80 reled glass powder fineness modulus (FM).
- Determine the fineness modulus (Fct) of mixtures of MG-30 and MG-80 powder recycled glass.

4.1.2. Methodology

A sieve analysis permitted to assess the particle size distribution of types of powdered recycled glass: MG-30 and MG-80. The analysis consisted of sieves #4, #8, #16, #30, #50, #100 and #200 with mesh sizes of 4.75 mm, 2.36 mm, 1.18 mm, 0.60 mm, 0.30 mm, 0.150 mm and 0.075 mm, respectively8. The total used mass of MG-30 and MG-80 recycled glass powder was 500 grams.

4.1.3. Results

4.1.3.1. Particle Distribution

Figure 18 shows the particle size distribution of MG30 and MG80 powdered recycled glass. MG80 displayed a more uniform particle size distribution compared to MG30. Table 7 presents the amount of MG30 and MG80 powdered recycled glass retained at each sieve. Eighty-five percent of MG30 particles were retained at sieves #40 and #60

with mesh sizes of 0.40 and 0.25 mm. Moreover, seventy-nine percent of MG80 particles were retained at sieves # 100 and # 200 with mesh sizes of 0.15 and 0.08 mm.

Table 7: Sieve Analysis

		MG30		MG80	
#	**Sieve, mm**	**Cumulative % Retained**	**Mass Retained, g**	**Cumulative % Retained**	**Mass Retained, g**
4	4.750	100.00	0.00	100.00	0
10	2.000	100.00	0.00	100.00	0
20	0.850	99.95	0.25	100.00	0
40	0.425	57.88	210.34	100.00	0
60	0.250	14.61	216.34	99.93	0.335
100	0.150	3.77	54.21	57.05	214.41
200	0.075	0.95	14.12	20.72	181.65
Pan			4.75		103.61
		Total	500.00	**Total**	500.00

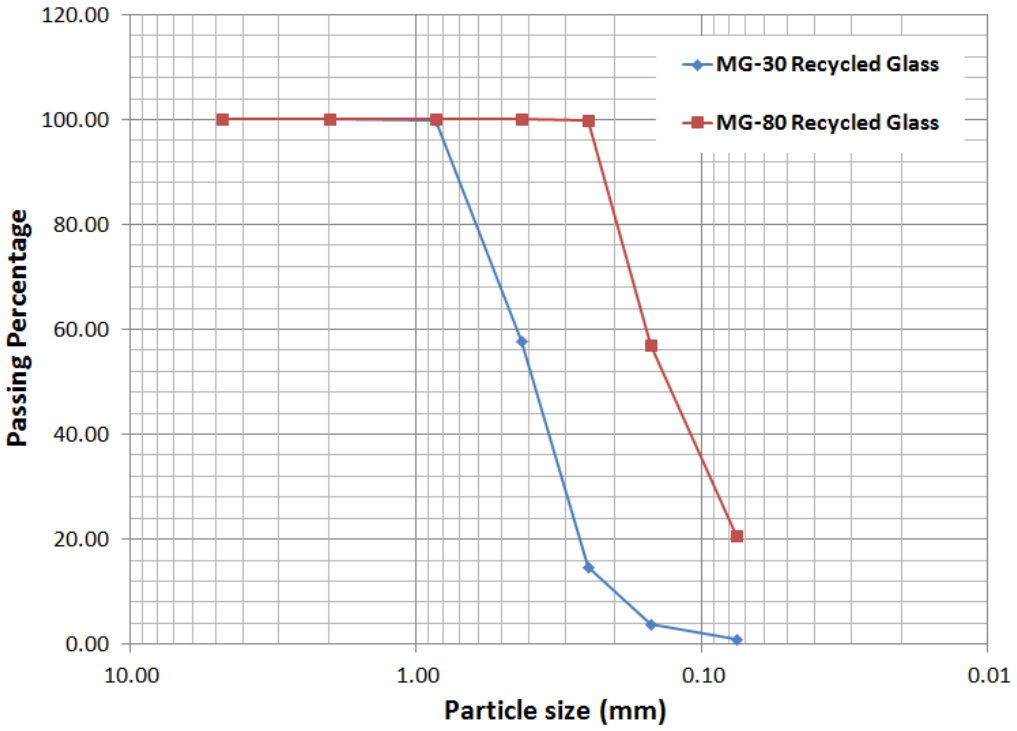

Figure 18: Passing percentage as a function of recycled glass particle size.

4.1.3.2. Fineness Modulus

The fineness modulus for MG30 and MG80 powdered recycled glass was obtained using Table 7 and Equations 4 and 5.

Retained Accumulated Percentage (% RA):

$$\% \mathbf{RA} = \mathbf{100}\ \% - \mathbf{Cumulative}\ \% \mathbf{Retained} \qquad \text{Equation 4}$$

Fineness Modulus (FM):

$$\mathbf{FM} = \sum \frac{\%\mathbf{RA}}{\mathbf{100}} \qquad \text{Equation 5}$$

MG-30 obtained a FM of **3.23**, while MG-80 obtained a FM of **1.22**.

4.1.3.3. Blends Fineness Modulus

Using Table 7, we calculated the fineness modulus of MG30-MG80 blends. Equation 6 allowed computing the blend passing percent at sieves 4, 10, 20, 40, 60, 100 and 200. An example of the calculation is shown for a blend of 50% MG-30 - 50% MG80.

$$\mathbf{Blend\ Passing}\ \%_{\mathbf{Sieve\ \#}} = \frac{(\%\ \mathbf{Passing\ MG30})_{\mathbf{Sieve\ \#}} * (\%\mathbf{MG30\ at\ blend}) + (\%\ \mathbf{Passing\ MG80})_{\mathbf{Sieve\ \#}} * (\%\mathbf{MG80\ at\ blend})}{\mathbf{100}} \qquad \text{Equation 6}$$

Example:

For sieve 100, at 50% MG30 - 50% MG80 blend, using Equation 6:

$$\textbf{Blend Passing } \%_{\textbf{Sieve 100}} = \frac{(\mathbf{3.77}\ \%)_{\textbf{Sieve 100}} * (\mathbf{50}\%) + (\mathbf{57.05}\%)_{\textbf{Sieve 100}} * (\mathbf{50}\%)}{\mathbf{100}} = \mathbf{30.412}\ \%$$

After calculating the blend passing percent at each sieve, we computed the fineness modulus using Equations 4 and 5. Table 8 summarizes the fineness modulus of the different MG30-MG80 blends. Figure 19 shows blends fineness modulus as function of blends MG30 percentage.

Table 8: MG-30 and MG-80 blends, fineness modulus (FM).

MG30	MG80	Fineness Modulus (FM)
0	**100**	3.77
5	**95**	3.13
10	**90**	3.03
15	**85**	2.93
20	**80**	2.83
25	**75**	2.73
30	**70**	2.63
35	**65**	2.53
40	**60**	2.43
45	**55**	2.33
50	**50**	2.23
55	**45**	2.13
60	**40**	2.03
65	**35**	1.92
70	**30**	1.82
75	**25**	1.72
80	**20**	1.62
85	**15**	1.52
90	**10**	1.42
95	**5**	1.32
100	**0**	1.22

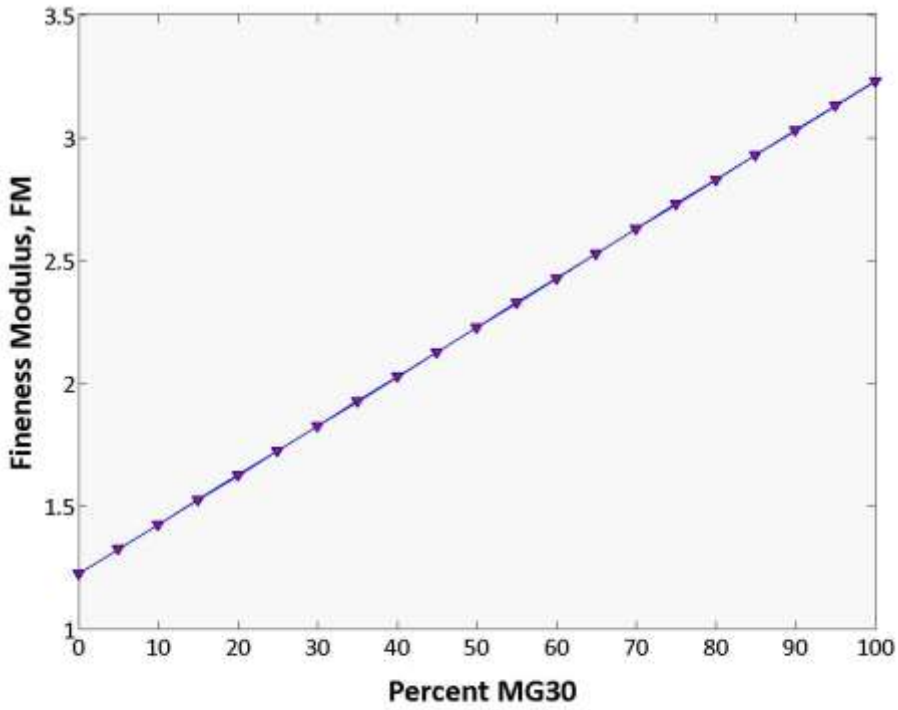

Figure 19: Blends fineness modulus as a function of MG30 percent.

4.1.3.4. Coefficient of uniformity

The coefficient of uniformity classifies the particle distribution grade of a soil and, in our case, of the powdered glass.[12] In this case we determined the particle grade distribution for both recycled glass powders, MG30 and MG80. The coefficient of uniformity, C_u is defined according to Equation 7.

$$\mathbf{C_u = \frac{D_{60}}{D_{10}}} \qquad \text{Equation 7}$$

where,

D_{60}, is the grain diameter at 60% passing,

D_{10}, is the grain diameter at 10 % passing by weight.

Using Figure 18, for MG30 we obtain:

$$\mathbf{C_{u_{MG30}} = \frac{D_{60-MG30}}{D_{10-MG30}} = \frac{0.43}{0.20} = 2.15}$$

This value defines MG30 as uniform fine sand. Moreover, MG80 grain diameter at 10% passing ($D_{10\text{-}MG80}$) cannot be defined from Figure 18, thus we can classify it as silty sand.

4.2. Scanning Electron Microscopy (SEM)

4.2.1. MG30 Recycled Glass

The JSM-6390 scanning electron microscope (UPRM Chemical Engineering Department) was used to obtain SEM images of the samples. Figure 20 shows MG30 recycled glass SEM images of a sample sintered at 725ºC for 25 minutes. In Figure 20a we can observe the MG30 recycled glass particle size distribution and void size. Figure 20b the coupling between two MG30 recycled glass beads at a magnification of 100X.

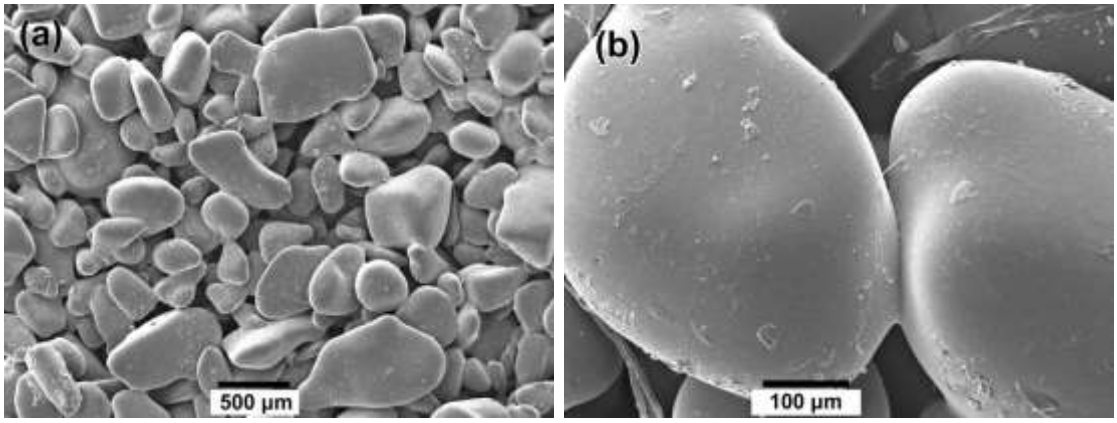

Figure 20: SEM images of MG30 recycled glass sintered at 725ºC for 25 minutes, (a) magnification of 40X, (b) magnification of 100X.

4.2.2. MG80 Recycled Glass

Figure 21 shows SEM images of MG80 recycled glass sintered at 750ºC for 25 minutes. In Figure 21a it is apparent that the MG80 glass possesses smaller voids than the MG30 one sintered with the same parameters. Furthermore, Figure 21b shows the particle size distribution of MG80 recycled glass.

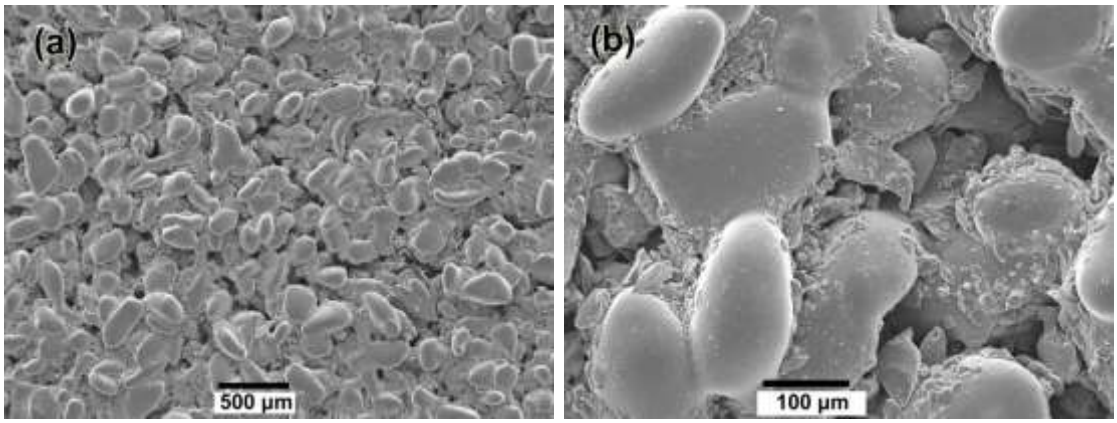

Figure 21: SEM images of MG80 recycled glass sintered at 750ºC for 25 minutes, (a) 40X, (b) 100X.

4.2.3. MG30 + TiO_2 Composites

MG30 recycled glass beads were mixed and sintered with different percentages of TiO_2. Figure 22 shows SEM images of MG30 recycled glass sintered with 1% TiO_2 at 800ºC for 20 minutes. We can observe the dispersion of TiO_2 particles on the MG30 particles at Figures 22a, 22b, and 22c.

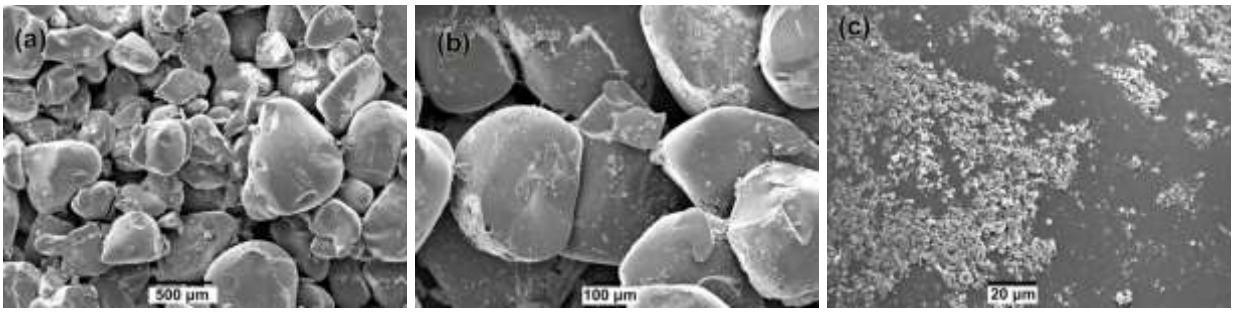

Figure 22: SEM images of MG30 recycled glass beads mixed with 1% TiO_2 sintered at 800ºC for 20 minutes, (a) 500 µm, (b) 100 µm, (c) 20 µm.

4.2.4. MG80 + TiO_2 Composites

Figure 23 shows SEM images of MG80 recycled glass sintered with 1% TiO_2 at 750ºC for 25 minutes. MG80 glass particles show a more spherical shape due the addition of TiO_2 particles. Furthermore, MG80+TiO_2 samples display smaller voids than MG30+TiO_2 samples.

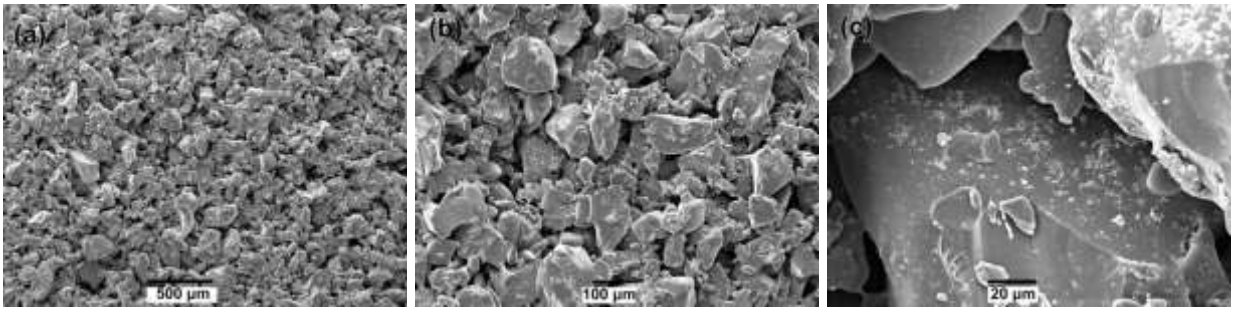

Figure 23: SEM images of MG80 recycled glass beads mixed with 1% TiO_2 sintered at 800ºC for 20 minutes, (a) 500 µm, (b) 100 µm, (c) 20 µm.

4.3. Surface Porosity

4.3.1. Objectives

- Obtain a performance map of the sintered recycled glass displaying how the filter surface porosity varies according to glass sintering temperature and time.
- Determine the effect of glass grain size on the resulting filter porosity.
- Assess the effect of different mass ratios of MG-30 and MG-80 recycled glass on the recycled glass surface porosity.
- Evaluate the effect of added TiO_2 particles on the recycled glass surface porosity.

4.3.2. Methodology

4.3.2.1. Sintering

4.3.2.1.1. Recycled Glass Powders

One gram samples of MG30 and MG80 recycled glasses were sintered at temperatures from 700ºC to 800ºC at 25ºC intervals for 10 to 30 minutes at 5 minutes intervals for porosity measurements.

4.3.2.1.2. Recycled Glass Blends

Blends of MG30 and MG80 (with a total mass of 1 gram) where sintered at 750ºC for 30 minutes. The percentage of MG30 in the blends ranged from 0 to 95%.

4.3.2.1.3. Recycled Glass with TiO_2 particles

One gram of recycled glass powders were mixed with TiO_2 particles. To prepare the mixtures containing from 1 to 0.5 % TiO_2, we used ethanol as solvent. The glass beads with TiO_2 were sintered at 750ºC for 30 minutes.

4.3.2.2. Polishing

After sintering, samples were mounted in epoxy resin and ground and polished with 60, 240,320, 400, 600, 800 and 1200 sand paper.

4.3.2.3. Microstructure Analysis

Micrographs of the sintered specimens were obtained using an optical microscope (Nikon Epiphot 200). These micrographs (obtained at 5x magnification) were examined using ImageJ to assess the percentage of porosity of the samples. Figure 24 shows an example of the analysis. The white regions in Figure 24b represent the sintered glass beads, while the black part represents the porosity after image correction. The image analysis software measured the black area and calculated the resulting porosity in percent area.

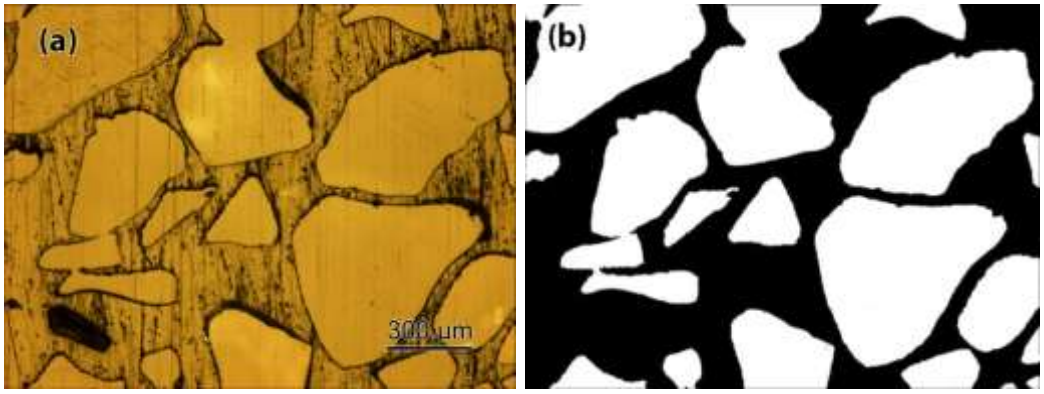

Figure 24: Samples micrographs analysis using ImageJ. (a) Original micrograph, (b) processed image used in the ImageJ analysis.

4.3.3. Results

4.3.3.1. MG30 Recycled Glass

A decrease in surface porosity becomes apparent as both sintering temperature and time increased (Figure 25). At this point it is important to recall that the MG30 samples contained a wide range of particle sizes, from 0.60 mm to 0.15 mm. Figure 26 present a surface plot that shows MG30 porosity changes according to sintering temperature and time. For MG30 was obtained a maximum porosity of 62% and a minimum porosity of 0% were obtained for the sintering parameter range used.

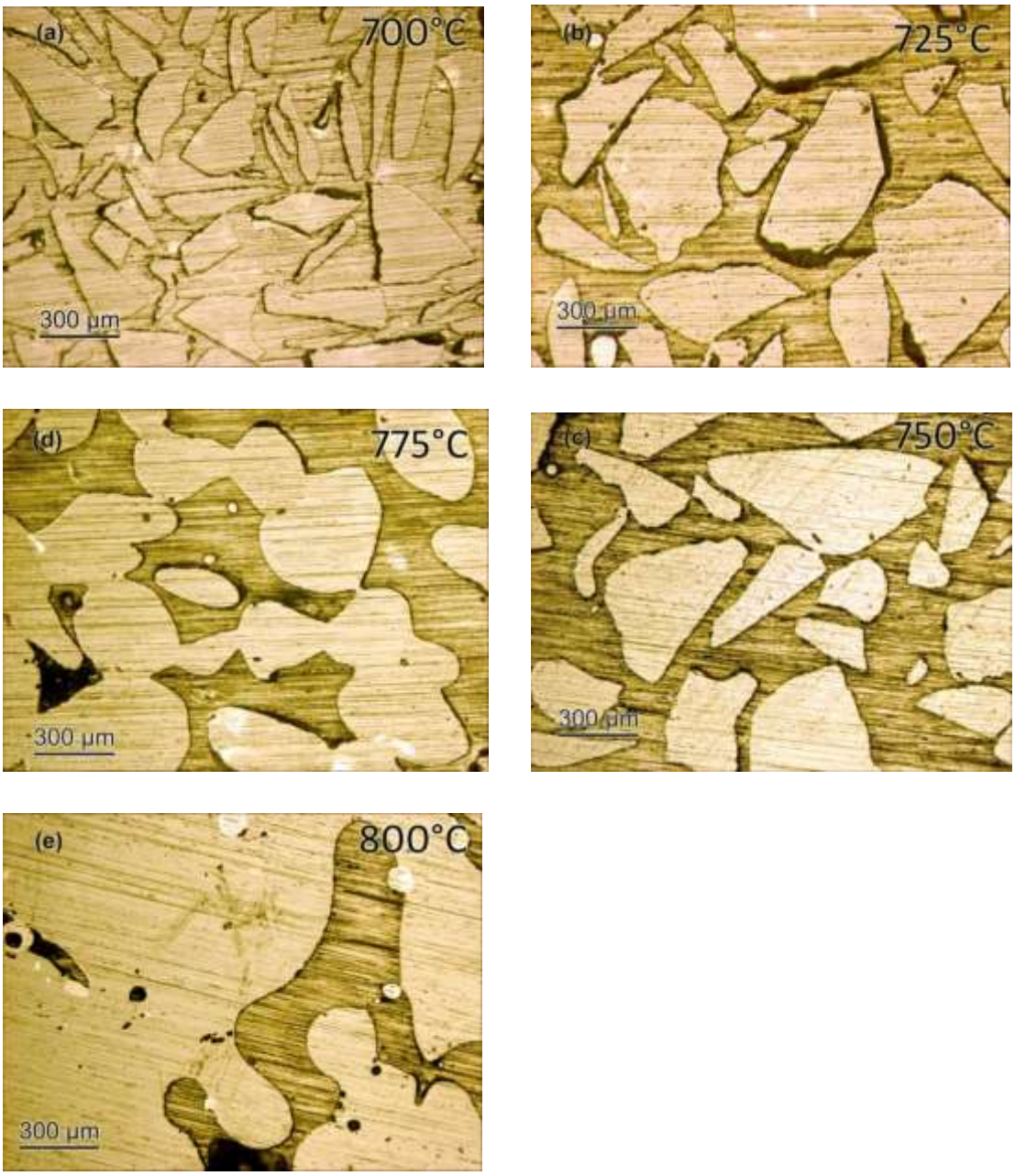

Figure 25: Sintered glass micrographs of 1 gram of MG-30 recycled glass sintered for 15 minutes at (a) 700ºC, (b) 725ºC, (c) 750ºC, (d) 775ºC, and (e) 800ºC.

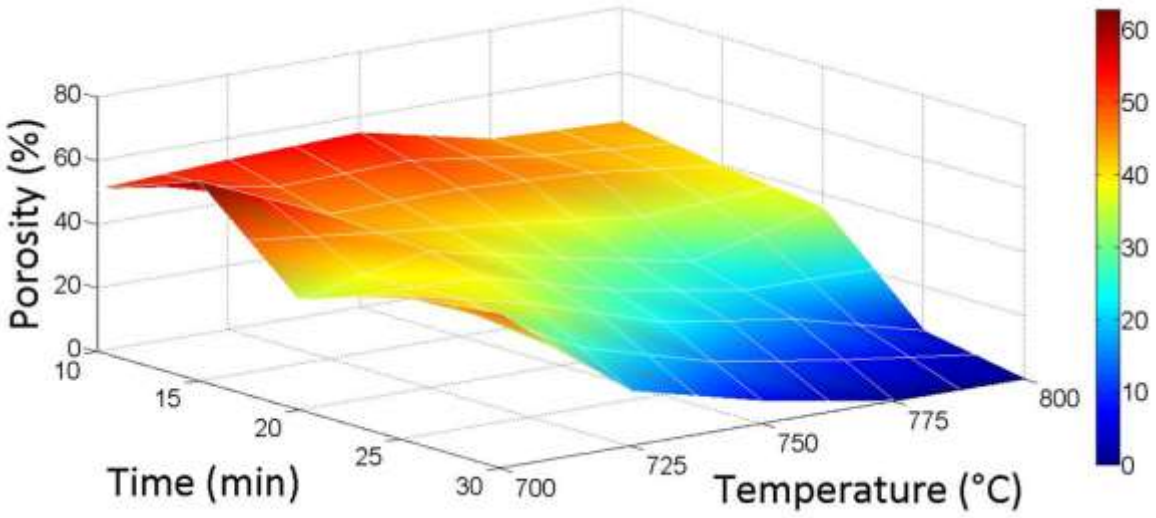

Figure 26: MG30 porosity as function of the sintering parameters.

4.3.3.2. MG80 Recycled Glass

Figure 27 reveals a decrease in the MG80 glass porosity as sintering temperature and time rise. Once again, it should be underscored that these MG80 samples contained particles with sizes ranging from 0.15 mm to 0.08 mm.

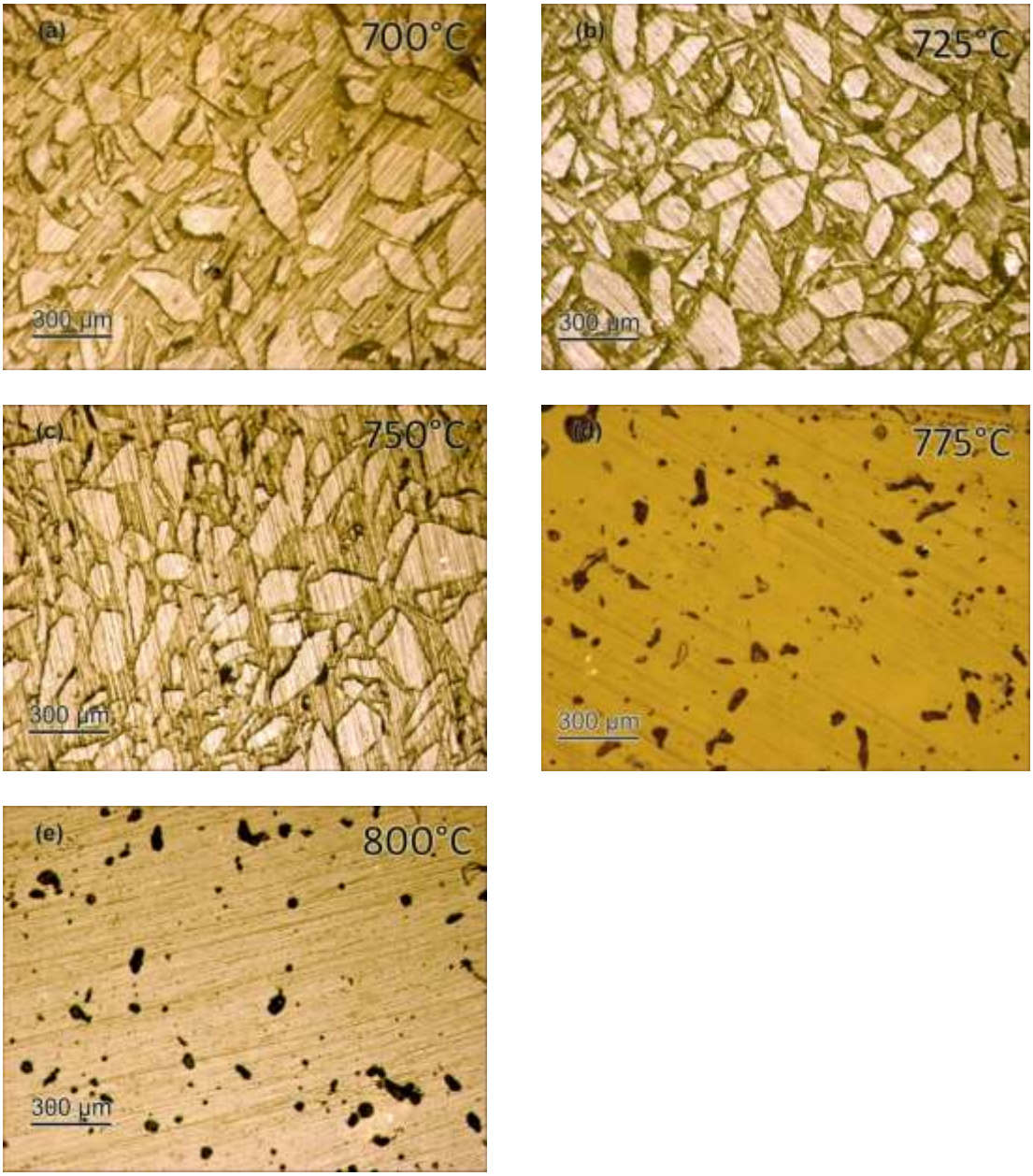

Figure 27: Surface micrographs of 1 gram of MG-80 recycled glass sintered for 15 minutes at (a) 700ºC, (b) 725ºC, (c) 750ºC, (d) 775ºC, and (e) 800ºC.

Figure 28 shows a surface plot of the MG-80 porosity as a function of sintering time and temperature. For this glass a maximum porosity of 68% and a minimum porosity of 4% were obtained for the sintering parameter range used. This demonstrates a pronounced effect of the sintering parameters and particle size on the resulting porosity.

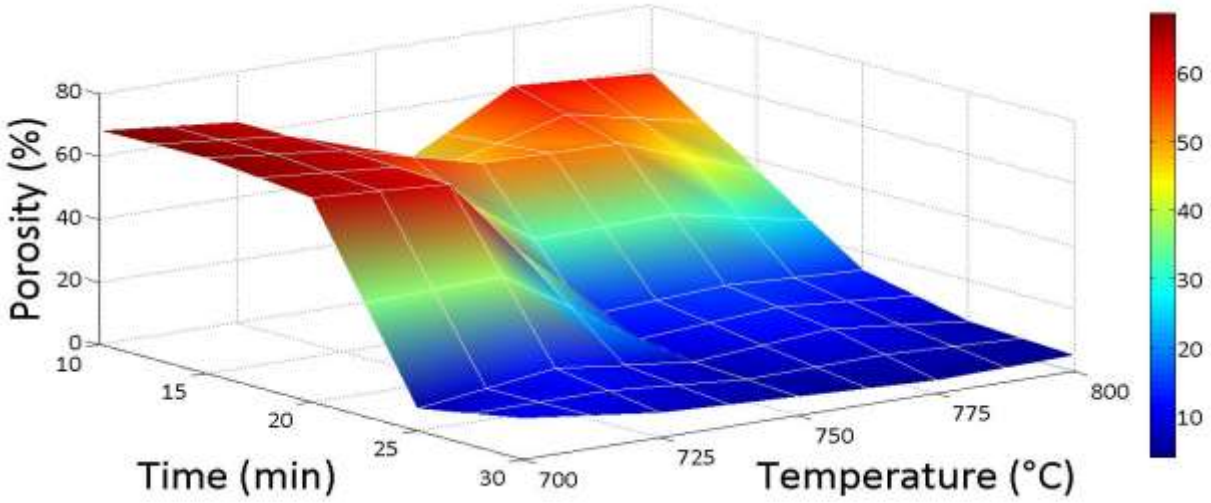

Figure 28: MG-80 porosity as function of sintering parameters.

4.3.3.3. MG30 + MG80 Blends

Less porosity is attained by adding MG80 particles, which is due to the smaller size of the MG80 particles that caused a 'fill-up' effect. This means that MG80 particles tended to fill the spaces among larger MG30 particles, and, thus, reduced that initial space among beads. Figure 29 shows micrographs of blends with 10% and 95% MG30 sintered at 750ºC for 30 minutes. Moreover, Figure 30 presents blends porosity changes as a function of MG30 percent in the samples. A uniform distribution is not apparent because the samples were sintered without prior sieving. As a consequence, one does not have a well-defined linear behavior. Equation 8 is the fit equation of Figure 30, with a R^2 of 85%.

Equation 8

$$\mathbf{Porosity}(\%)_{\mathbf{Blends}} = \mathbf{7.46} * \mathbf{exp}(\mathbf{5.495} * \mathbf{10^{-3}} * \mathbf{MG30}(\%) + \mathbf{3.634} * \mathbf{10^{-6}} * \mathbf{exp}(\mathbf{0.1564} * \mathbf{MG30}(\%))$$

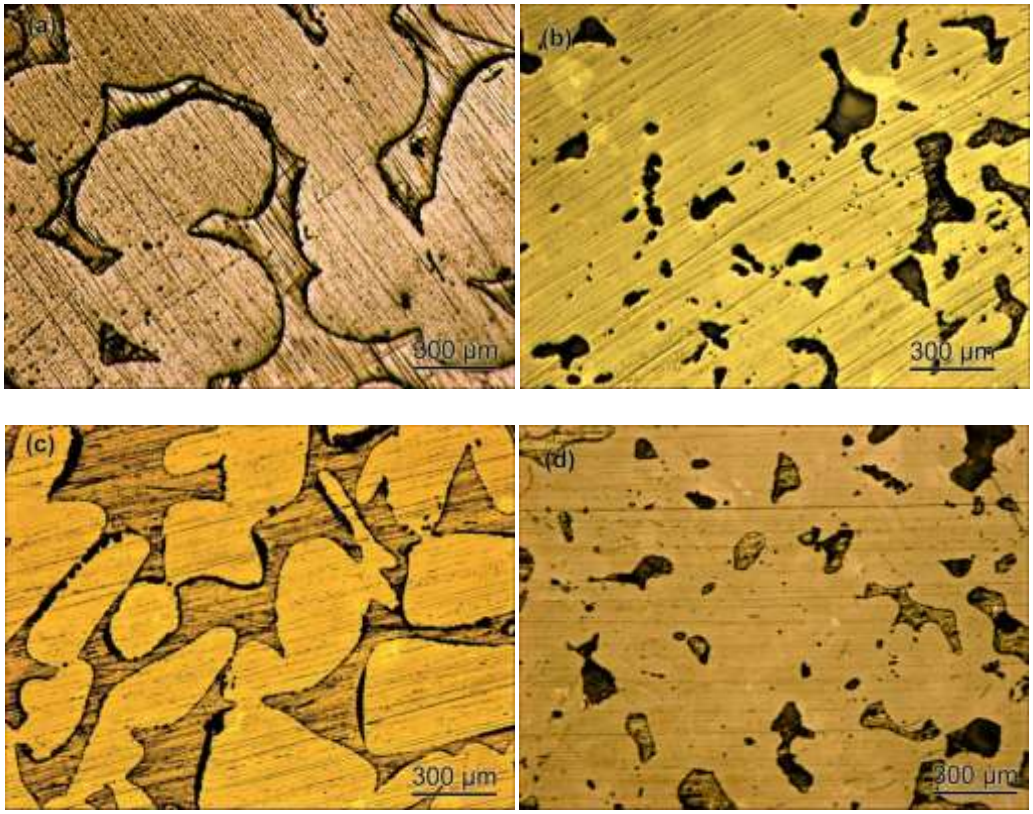

Figure 29: MG30-MG80 blend with (a) 85% MG30 recycled glass, (b) 10% MG30, (c) 100% MG30, and (d) 100% MG80, sintered at 750ºC for 30 minutes.

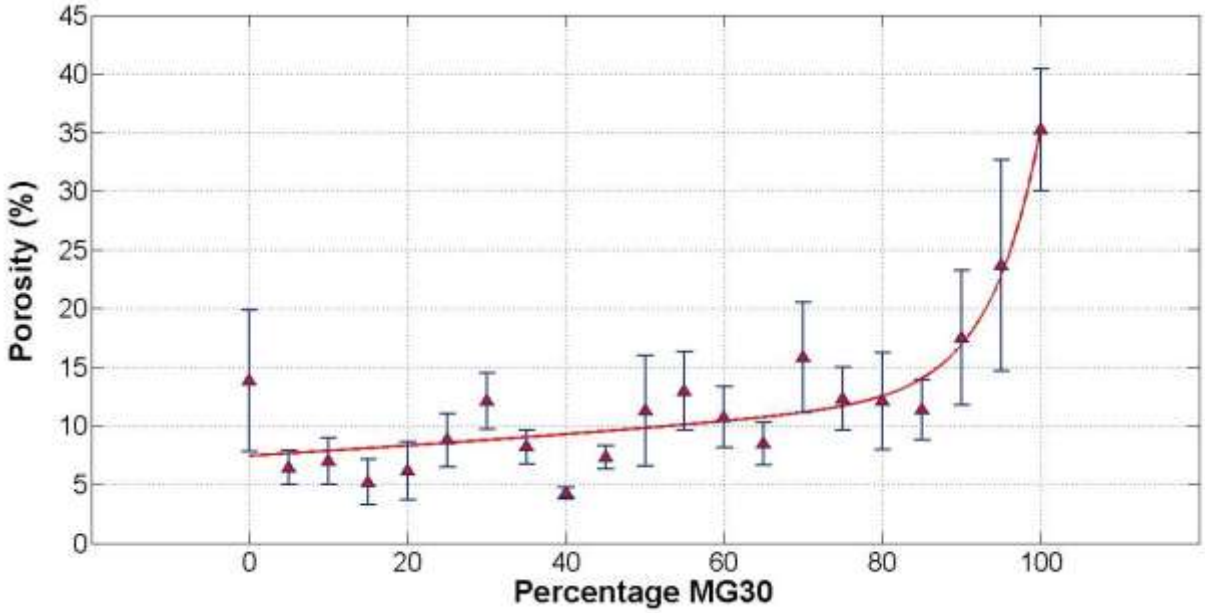

Figure 30: Porosity as a function of the amount of MG30 in each blend.

4.3.3.4. MG30 and MG80 glasses sintered with TiO_2 particles

Figure 31 and 32 correspond to micrographs of MG30 and MG80 respectively, sintered with different amounts of TiO_2. It is apparent that the addition of TiO_2 has not caused significant changes in the recycled glass porosity. Figure 33 and 34 summarizes the measured porosity with respect to the added TiO_2 percentage to MG30 and MG80. The addition of TiO_2 particles decreased MG30 porosity till 1 wt% TiO_2 were porosity increases. Moreover, a significant reduction in MG80 porosity resulted with the addition of TiO_2 particles. This behavior can be attributed to the fact that the MG80 beads and TiO_2 particles had similar particle size. Meanwhile we can observe the same behavior presented with MG30 where MG80 porosity increases with the addition of 1 wt% TiO_2. At 1 wt% recycled glass sintering mechanisms, of surface and grain boundary diffusion,

are decreased by the presence of TiO_2 particles. Equation 9 and 10 are the fitted equations of Figures 33 and 34, respectively. Both equations are good fits of the data with R^2 values of 91% and 98% respectively.

Equation 9

$$\mathbf{Porosity}\ (\%)_{\mathbf{MG30+TiO2}} = \mathbf{36.86} * \mathbf{exp}\left(\mathbf{0.1305} * \mathbf{TiO_2}\ (\%)\right) - \mathbf{1.537} * \mathbf{exp}(\mathbf{-29.49}\ * \mathbf{TiO_2}\ (\%))$$

Equation 10

$$\mathbf{Porosity}\ (\%)_{\mathbf{MG80+TiO2}} = -\mathbf{18.22} * \mathbf{TiO_2}(\%)^{\mathbf{3}} + \mathbf{53.74} * \mathbf{TiO_2}\ (\%)^{\mathbf{2}} - \mathbf{41.66} * \mathbf{TiO_2}\ (\%) + \mathbf{13.47}$$

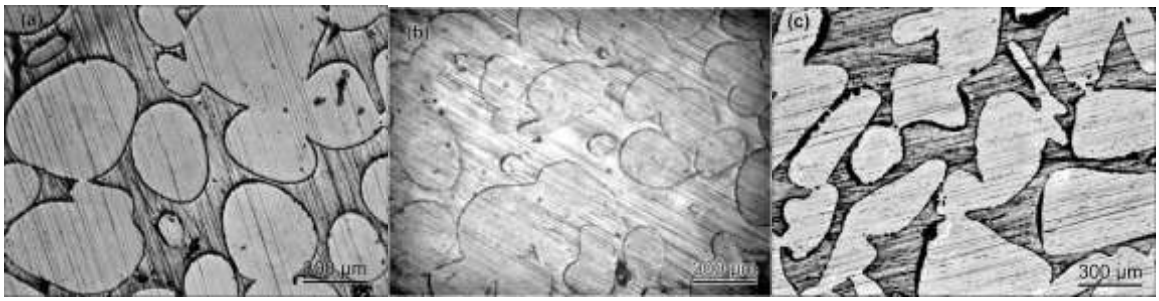

Figure 31: Optical micrographs of MG30 recycled glass with (a) 0.7% TiO_2, (b) 1% TiO_2, and (c) 0% TiO_2. All samples were sintered at 750ººC for 30 minutes.

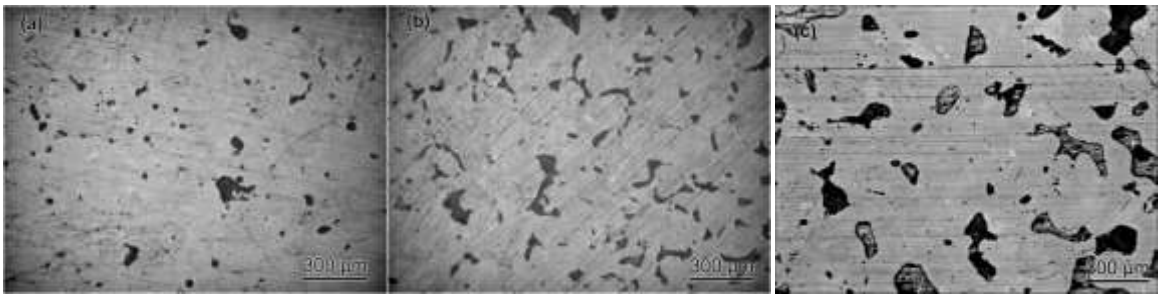

Figure 32: Optical micrographs of MG30 recycled glass with (a) 0.7% TiO_2, (b) 1% TiO_2, and (c) 0% TiO_2. All samples were sintered at 750ºC for 30 minutes.

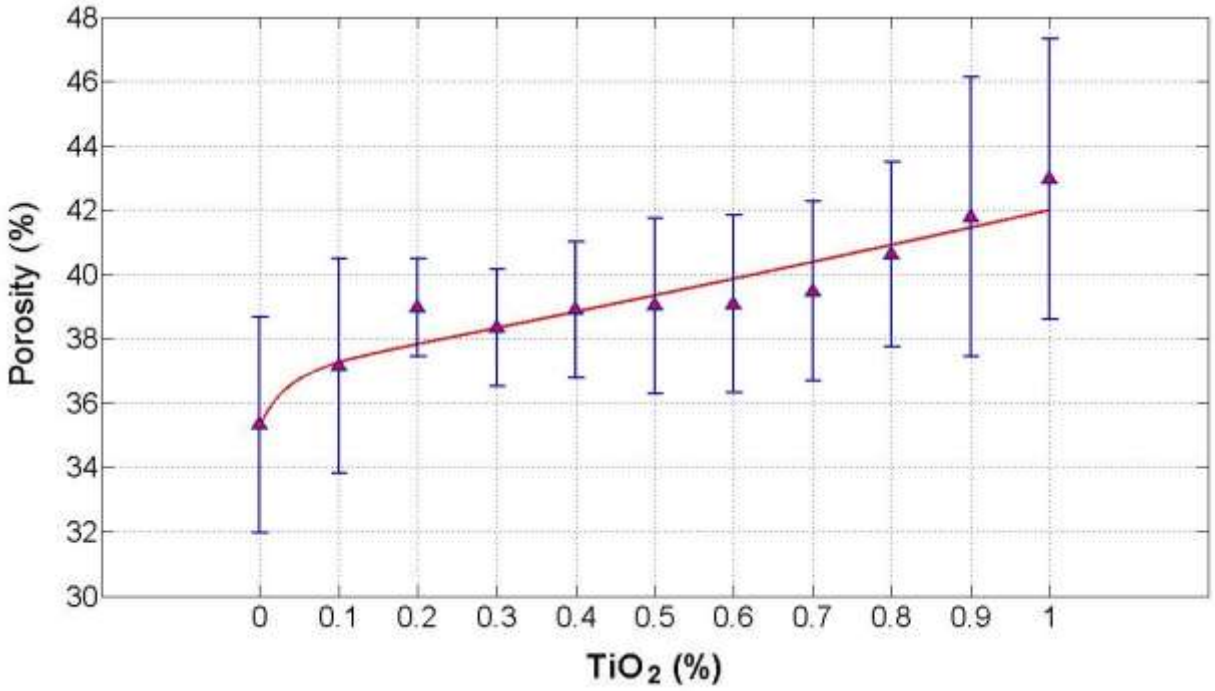

Figure 33: Recycled glass porosity changes according to TiO_2 percentage in MG30.

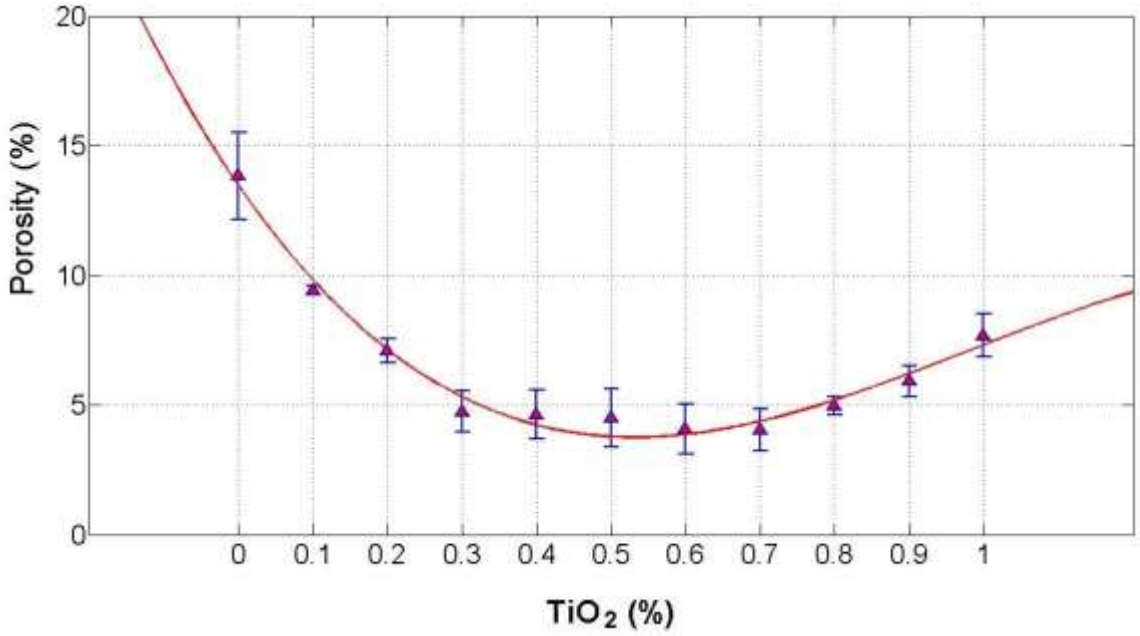

Figure 34: Recycled glass porosity changes according to TiO_2 percent present in MG80.

4.3.3.5. MG30 + MG80 blends sintered with TiO_2 particles

Figure 35 summarizes recycled glass blends sintered with 1% of TiO_2. We can observe that porosity decreases with the addition of 1% TiO_2 for blends of 0 to 70% MG30. In this case, the dominant particles are from MG80 recycled glass (smaller ones), thus porosity will decrease because the TiO_2 will fill the small voids created by MG80 particles. For contents above 70% MG30, a sharp increase in samples porosity is apparent. Here, porosity is directly affected by MG30 particles, thus the addition of 1 wt% increases the porosity of samples due the decrease in the sintering mechanisms of surface and grain boundary diffusion. Equation 10 is the fitted equation shown in Figure 35 with an R^2 of 83%.

Equation 10

$$\mathbf{Porosity}_{\mathbf{Blends+TiO_2}} = \mathbf{3.327} * \mathbf{10^{-5}} * \mathbf{MG30}(\%)^{\mathbf{3}} + \mathbf{3} * \mathbf{10^{-3}} * \mathbf{MG30}(\%)^{\mathbf{2}} - \mathbf{0.291} * \mathbf{MG30}(\%) + \mathbf{9.818}$$

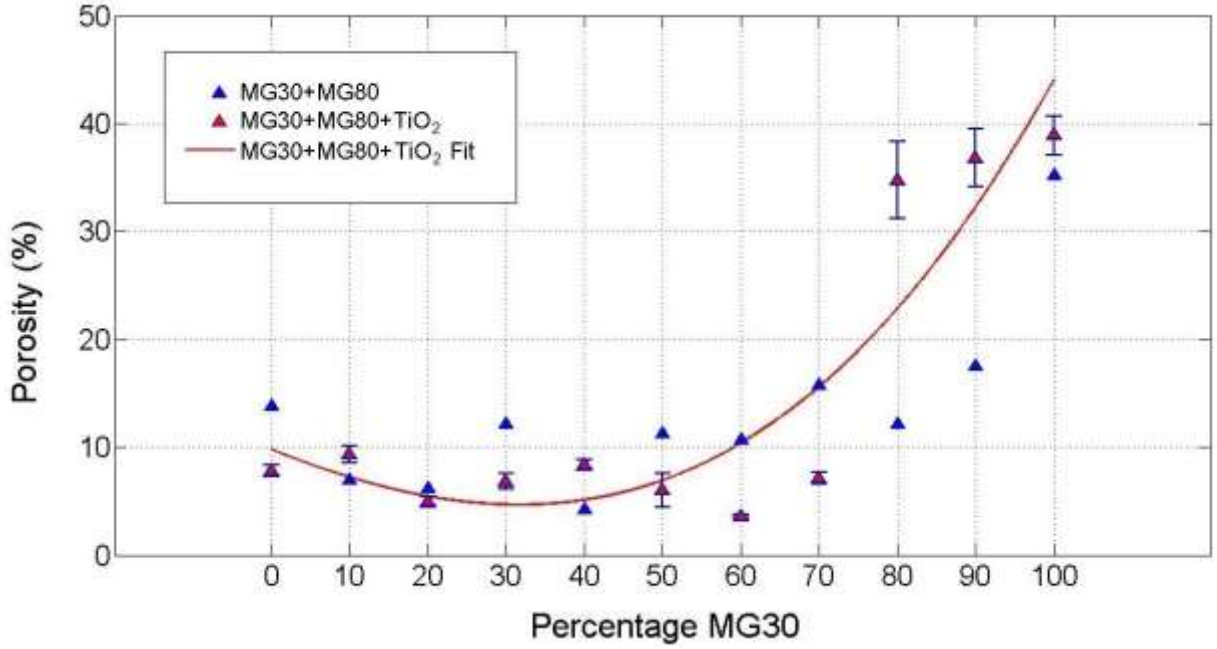

Figure 35: MG30-MG80 blends porosity changes by the addition of 1% TiO_2. Samples were sintered at 750ºC for 30 minutes.

4.4. Percolation

4.4.1. Objectives

- Obtain a map of filter percolation performance as a function of sintering temperature and time.
- Assess the effect of the recycled glass particle size on the filter percolation.
- Corroborate the inverse relationship between both sintering parameters and the filter percolation.
- Measure the percolation through MG30 + MG80 blends.
- Measure filters percolation as a function of the addition TiO_2 particles.

4.4.2. Methodology

4.4.2.1. Sintering

4.4.2.1.1. MG30 and Mg80 Recycled Glass Powders

For the percolation measurements, 30 g of MG30 and MG80 recycled glass were sintered from 700ºC to 800ºC at 25ºC intervals for 10 to 30 minutes at 5 minutes intervals.

4.4.2.1.2. MG30 and MG80 Recycled Glass Blends

Blends of MG30 + MG80 (with a total mass of 30 grams) were sintered at 750ºC for 30 minutes. The percent of MG30 in the blends ranged from 0 to 95% for this percolation study.

4.4.2.1.3. MG30 and MG80 Recycled Glass Powders with TiO_2 particles

Thirty grams of recycled glass powders where mixed with TiO_2 particles. To prepare the mixtures containing from 0.5% to 1% TiO_2, we used ethanol as solvent. The glass beads with TiO_2 were sintered at 800ºC for 20 minutes for the percolation measurements.

4.4.2.2. Analysis

Figure 36 shows a schematic of the percolation apparatus used to assess the sintered filters percolation characteristics. It was designed to obtain a one directional water flux through sintered recycled glass samples. The design consisted of a water inlet pipe connected to a clear-colored cube. The sintered samples sit at the cube bottom surface. This surface was connected to a pipe and valve where the water-outlet flux is controlled. Finally, a water container placed below the system allowed measuring the water volume change through the samples. Percolation (Equation 11) was determined by recording the elapsed time (Δt, in seconds) to obtain a water volume of 600 millimeters at the water container (ΔV_w, in millimeters). Figure 37 shows the used percolation apparatus.

$$\mathbf{P_{flux}}\left(\frac{\mathbf{ml}}{\mathbf{s}}\right) = \frac{\mathbf{\Delta V_w}}{\mathbf{\Delta t}} \qquad \text{Equation 11}$$

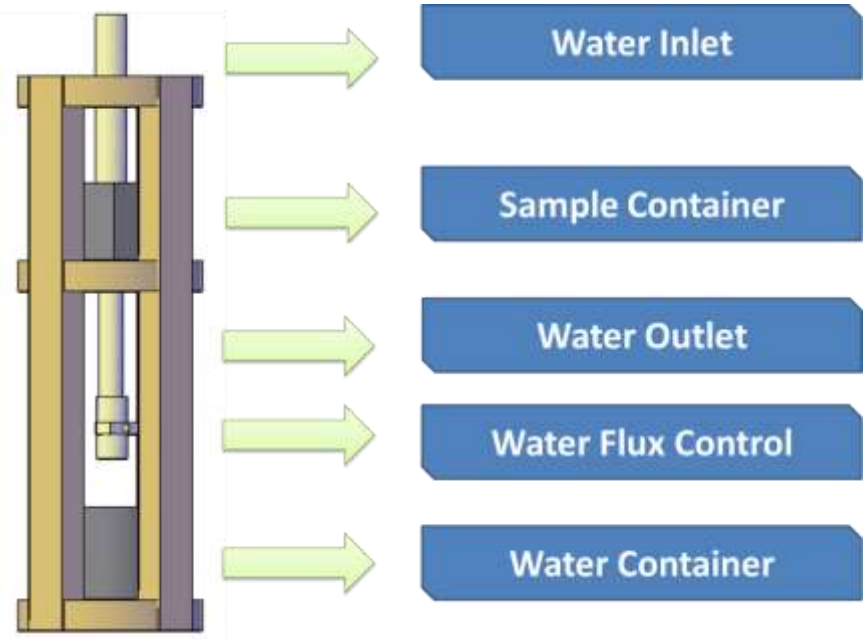

Figure 36: Schematic of percolation apparatus.

Figure 37: Percolation apparatus.

4.4.3. Results & Discussion

4.4.3.1. Effects on MG30 and MG80 Recycled Glass

Figure 38 shows optical micrographs of (a) MG30 and (b) MG80 filters sintered at 750ºC for 20 minutes. One can clearly infer that particle size played a major role in the filters porosity. For the same sintering parameters, MG-30 showed bigger voids than MG80.

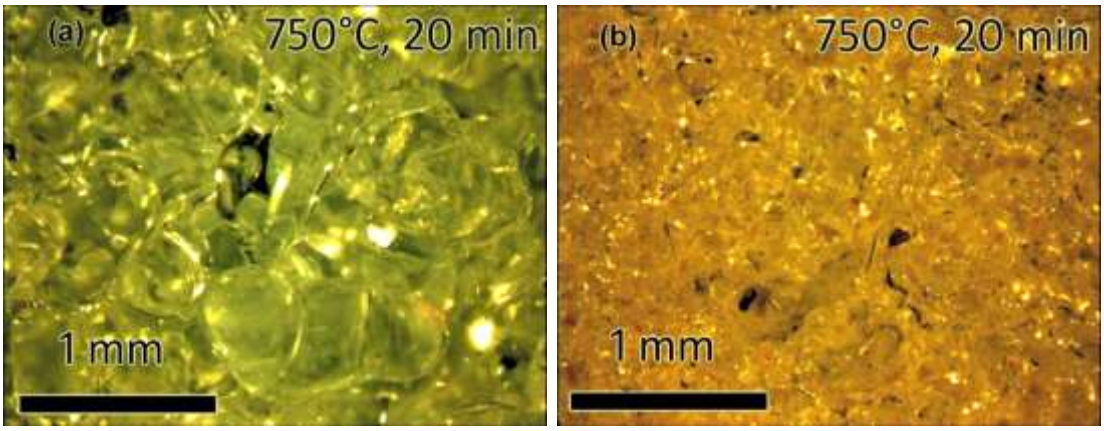

Figure 38: Surface micrographs of: (a) MG-30, (b) MG-80 percolation samples sintered at 750ºC for 20 min.

Fragile MG-30 samples were obtained at low sintering parameters, i.e. from 700ºC to 725ºC degrees and for 10 to 15 minutes. Similarly, fragile MG-80 samples resulted at sintering temperatures from 700ºC to 775ºC for times from 10 to 15 minutes. Figures 39 and 40, show MG-30 and MG-80 percolation as a function of sintering temperature and time. MG-30 samples highest and lowest percolation values were 55 ml/s and 3 ml/s, respectively. Moreover, MG-80's highest and lowest percolation values were 18 ml/s and 0.63 ml/s, respectively.

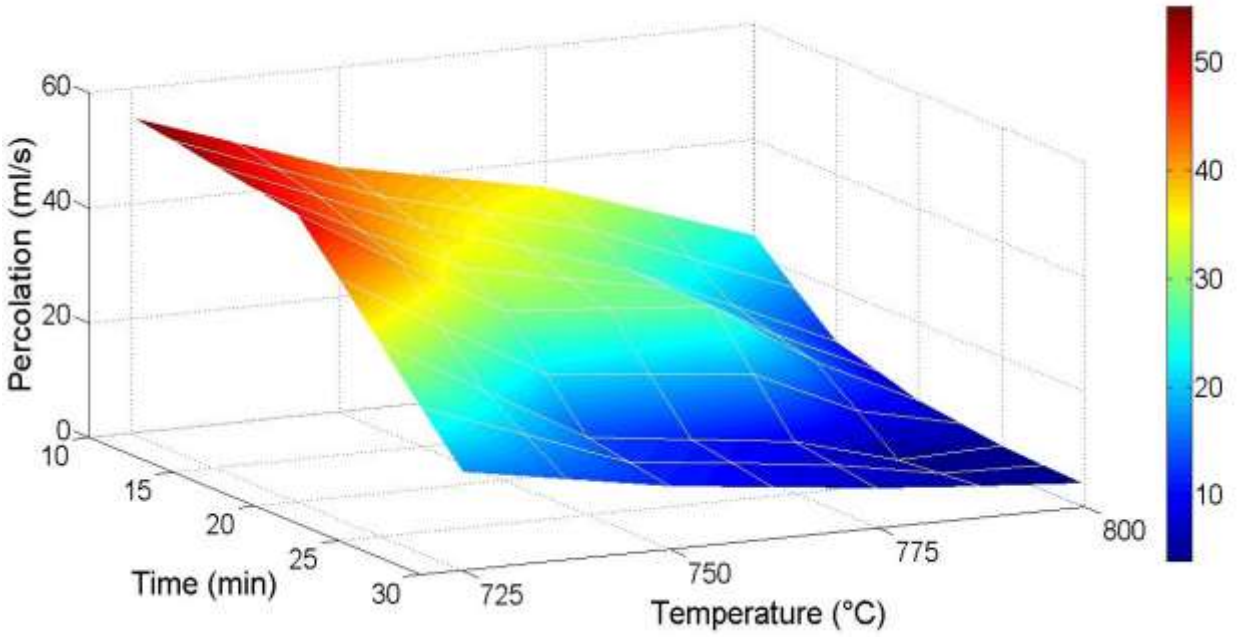

Figure 39: MG-30 percolation as a function of sintering parameters.

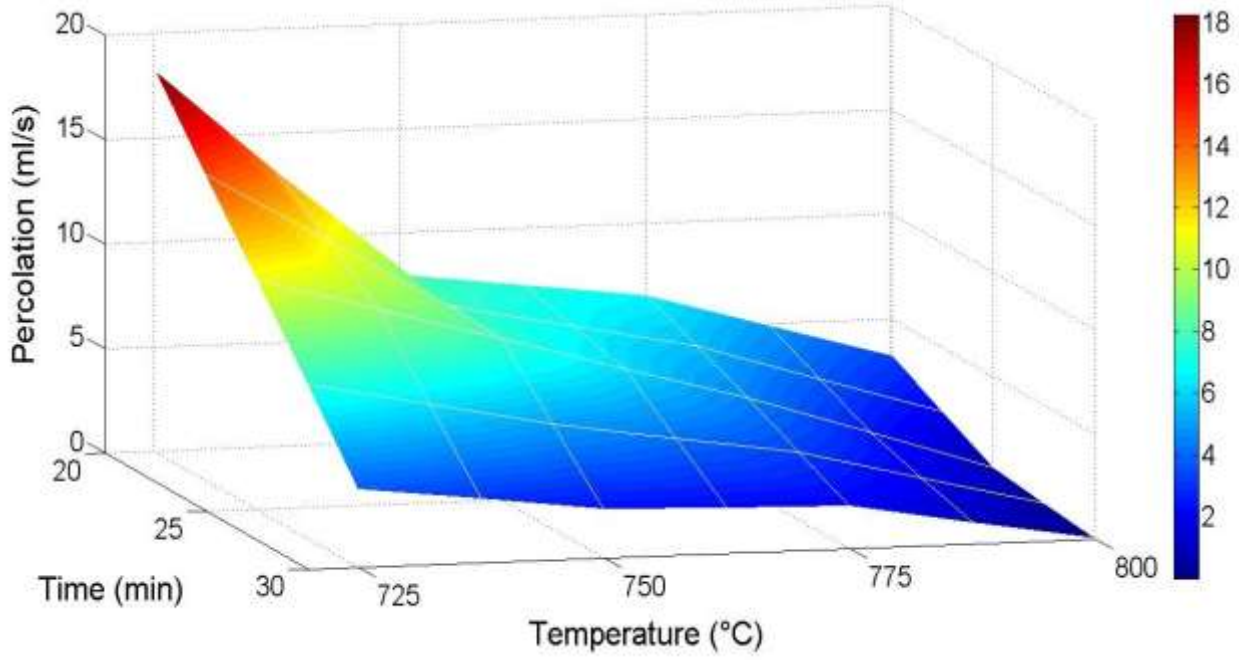

Figure 40: MG-80 percolation as a function of sintering parameters.

4.4.3.2. MG30 + MG80 Recycled Glass Blends

In these glass blends an increase in percolation is evident for increasing amounts of MG30. Figure 41 shows the percolation values of blends with different percentages of MG30. A direct relationship between blends MG30 percentage with percolation values is apparent. Moreover, the percolation values remains constant at blends between 0 and 40% MG30. One should recall that MG80 particles are smaller than MG30 and located themselves between MG30 particles, decreasing the samples percolation. These samples were sintered at 750ºC for 30 minutes. Equation 12 (R^2 of 82%) is the fitted equation for Figure 41.

$$\textbf{Percolation}\left(\frac{\textbf{ml}}{\textbf{s}}\right) = \mathbf{1.631} * \mathbf{exp}(\mathbf{0.0163} * \mathbf{MG30}\ (\%)) \qquad \text{Equation 12}$$

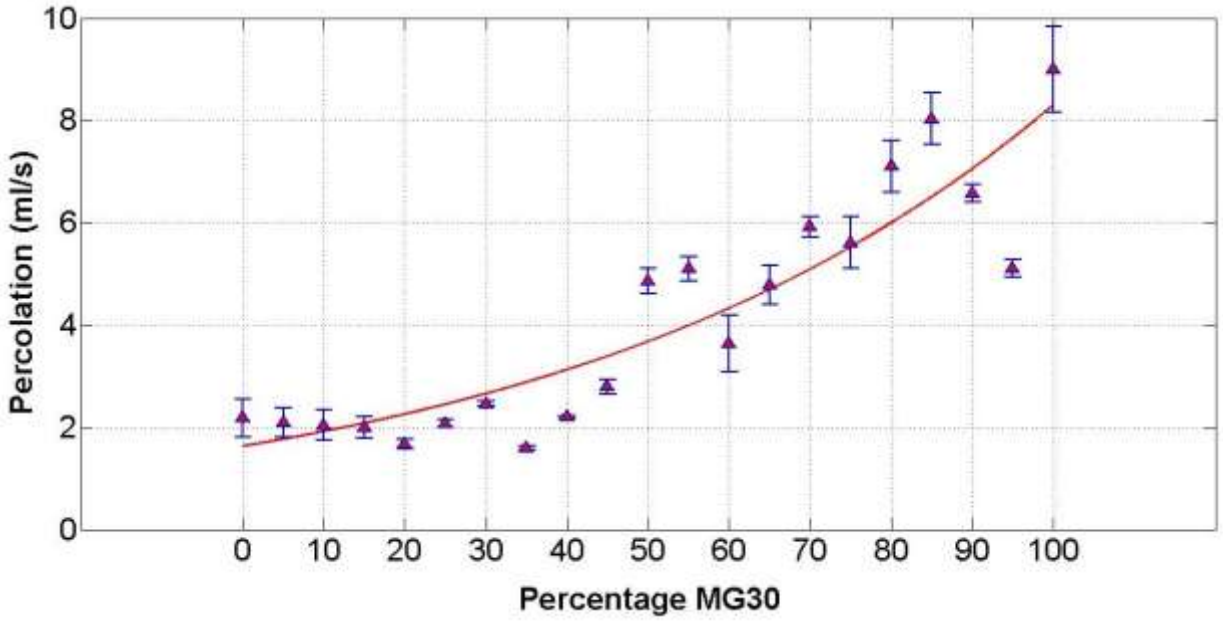

Figure 41: Blends Percolation changes according to MG30 percentage.

4.4.3.3. MG30 Recycled Glass Powder with TiO_2 particles

The presence of TiO_2 decreased the percolation properties of MG30 filters. Figure 42 shows the percolation values of MG30 recycled glass with different percentages of TiO_2. Percolation values decreased from 3.7 to 1.61 ml/s. This behavior can be attributed to the smaller TiO_2 particles which locate themselves between MG30 particles, thus decreasing the filter percolation properties. The presence of TiO_2 particles decreased MG30 sintering mechanisms, obtaining fragile samples at low sintering parameters (from 700°C to 775°C for 10 to 20 minutes). In order to obtain non-fragile samples, we sintered MG30-TiO_2 at 800ºC for 20 minutes. Moreover, we expect the same behavior for samples sintered at other temperatures: the presence of TiO_2 particles in filters will decrease samples percolation flux. Equation 13 (R^2 = 97%) is the equation for the fitted curve in Figure 42.

$$\mathbf{Percolation}\left(\frac{\mathbf{ml}}{\mathbf{s}}\right)_{\mathbf{MG30+TiO_2}} = \mathbf{3.756} * \mathbf{exp}\left(-\mathbf{1.008} * \mathbf{TiO_2}(\%)\right) \qquad \text{Equation 13}$$

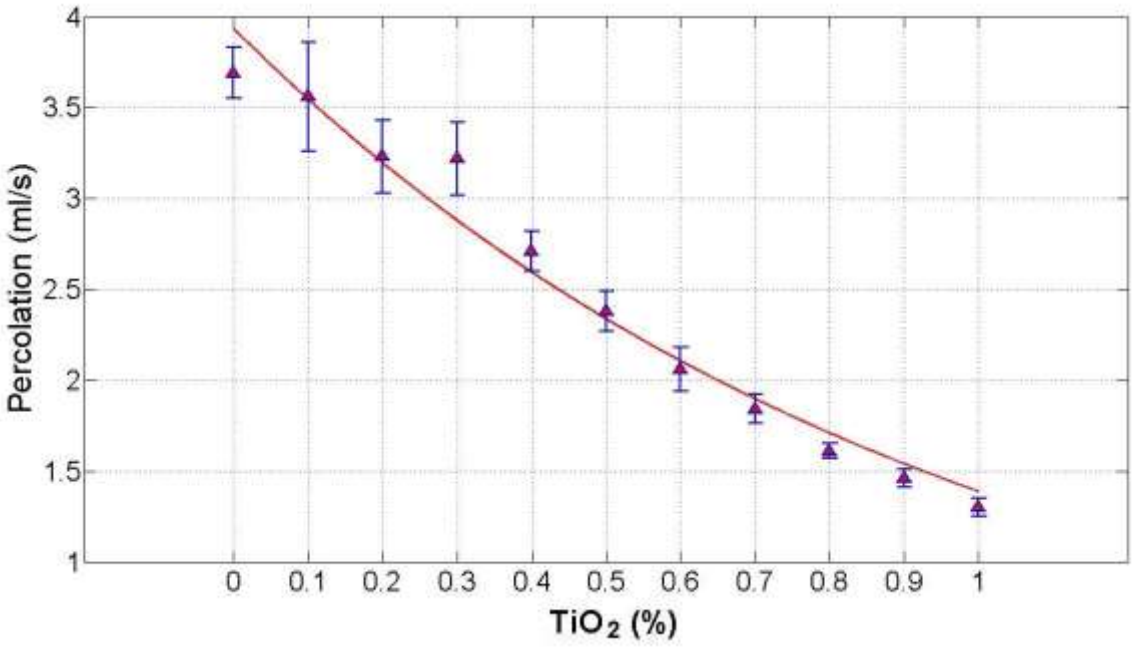

Figure 42: Percolation of MG30 recycled glass sintered with TiO_2 particles at 800ºC for 20 minutes.

4.4.3.4. MG80- Recycled Glass Powder with TiO_2 particles

An inverse relationship between samples percolation with the amount of TiO_2 is apparent. Figure 43 shows the percolation values of MG80 recycled glass as a function of the TiO_2 content. Percolation values decreased a 78%, from 3.26 to 0.72 ml/s, by the addition of TiO_2. MG80 percolation values decreased more dramatically than MG30's due the presence of TiO_2 particles. As explained before, TiO_2 particles will locate themselves between MG80 particles, thus decreasing the filter percolation properties. These samples were sintered at 800°C for 20 minutes. As happened with the MG30, the addition of TiO_2 decreased MG80 sintering mechanisms; thus higher temperatures were required to obtain non-fragile samples. Equation 14 (R^2 = 99%) is the equation of fitted curve shown in Figure 43.

$$\mathbf{Percolation}\left(\frac{\mathbf{ml}}{\mathbf{s}}\right)_{\mathbf{MG80+TiO_2}} = \mathbf{3.249} * \mathbf{exp}\left(-\mathbf{3.044} * \mathbf{TiO_2}(\%)\right) \qquad \text{Equation 14}$$

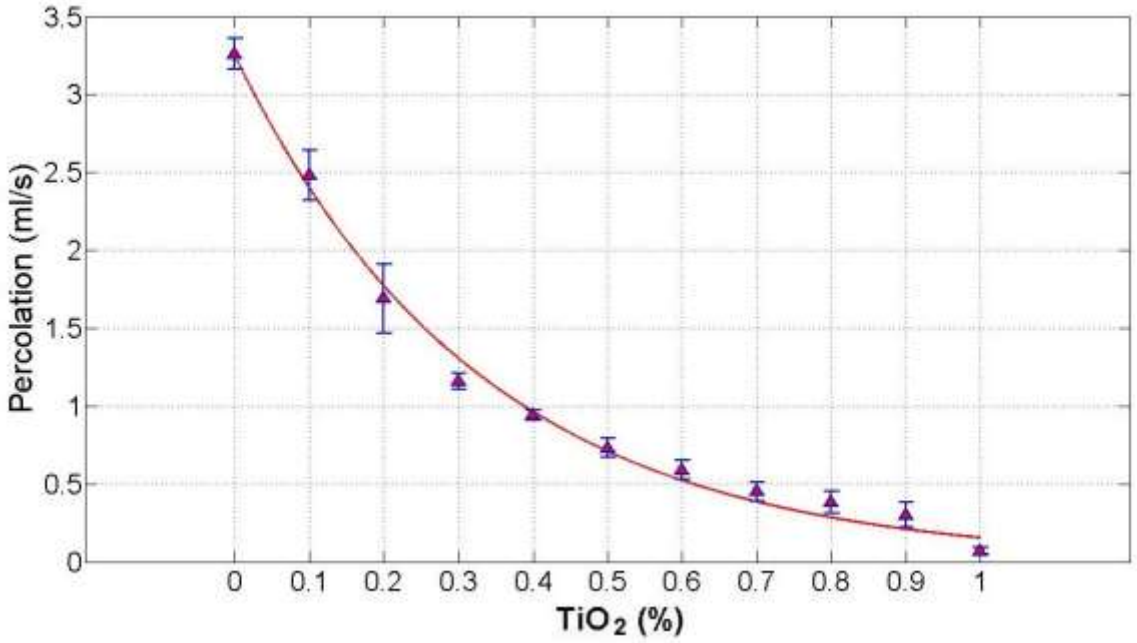

Figure 43: Percolation of MG80 recycled glass sintered with TiO_2 particles at 800ºC for 20 minutes.

Chapter 5: Mechanical Analysis

5.1. Compression Test

5.1.1. Objectives

- Assess MG-30 and MG-80 sintered filters compression characteristics as function of sintering time and temperature.
- Measure MG-30 + MG-80 mixtures compression characteristics.
- Determine the effect of TiO_2 particles on the filters compression characteristics.

5.1.2. Specifications

5.1.2.1. Specimens Dimensions

Compression samples had a length of 17.80 mm, width of 17.80 mm, and thickness of 6.35 mm.

5.1.2.2. Test

The MG30 and MG80 samples were loaded under compression until fracture occurred. The maximum strength of the MTS 8800 compression machine (shown in Figure 44) was 25 kN. The machine was operated with a loading rate of 0.127 mm/min according to the ASTM C1424-04: *Standard Test Method for Monotonic Compressive Strength of Advanced Ceramics at Ambient Temperature*. The samples compressive strength was obtained by dividing the fracture force by the specimen's surface area (Equation 15).

Figure 44: MTS compression test machine.

$$\boldsymbol{\sigma = \frac{F_{Max}}{A_{surface}}} \qquad \text{Equation 15}$$

5.1.3. Results

5.1.3.1. MG30 Recycled Glass

Figure 45 shows the MG30 compressive strength. At low temperatures (from 700º to 750ºC) for 10 to 25 minutes we obtained fragile samples. Furthermore, an increase in compressive strength for sintering temperatures from 775º to 800ºC for 10 to 30 minutes is evident. The maximum compressive strength obtained was 80 MPa for samples sintered from 750ºC to 800ºC for 30 minutes.

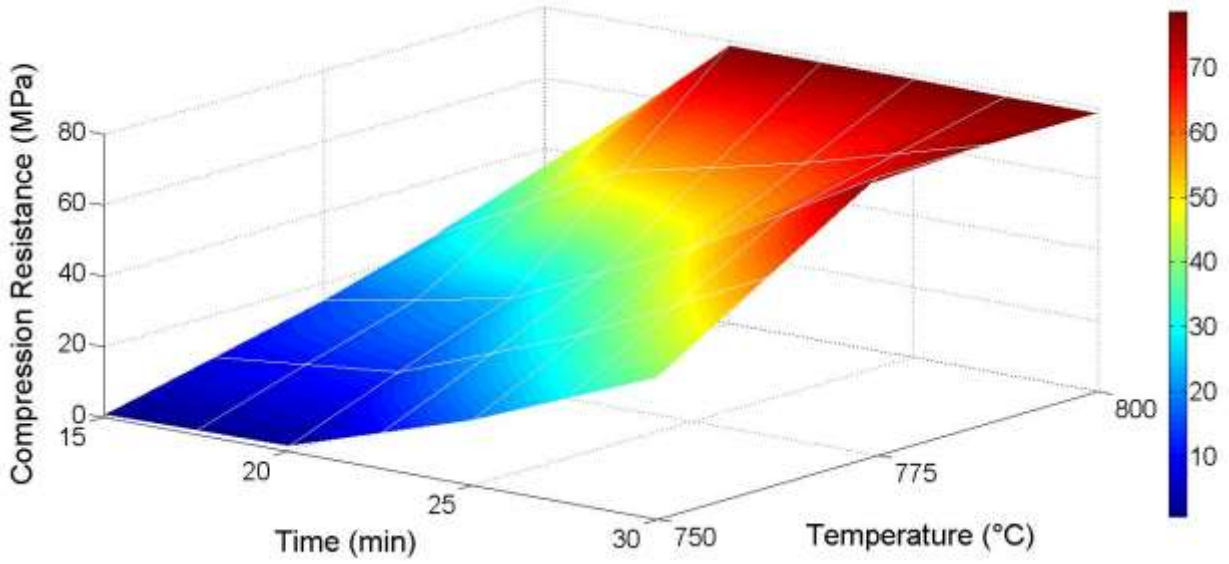

Figure 45: MG30 compressive strength as function of the sintering parameters.

5.1.3.2. MG80 Recycled Glass

Figure 46 shows the MG80 compressive strength behavior. Fragile samples resulted at temperatures from 700º to 725ºC for 10 to 25 minutes. Moreover, an increase in the compressive strength is visible from specimens sintered from 750º to 800ºC for 10 to 30 minutes. In this case the maximum compressive strength obtained was 80 MPa for samples sintered from 775ºC to 800ºC for 20 to 30 minutes. MG80 samples showed higher compressive strength than MG30 samples with the same sintering parameters. MG80 presented smaller voids compared to MG30 at the same sintering parameters, which implicates less the available space for deformation and higher compression resistance.

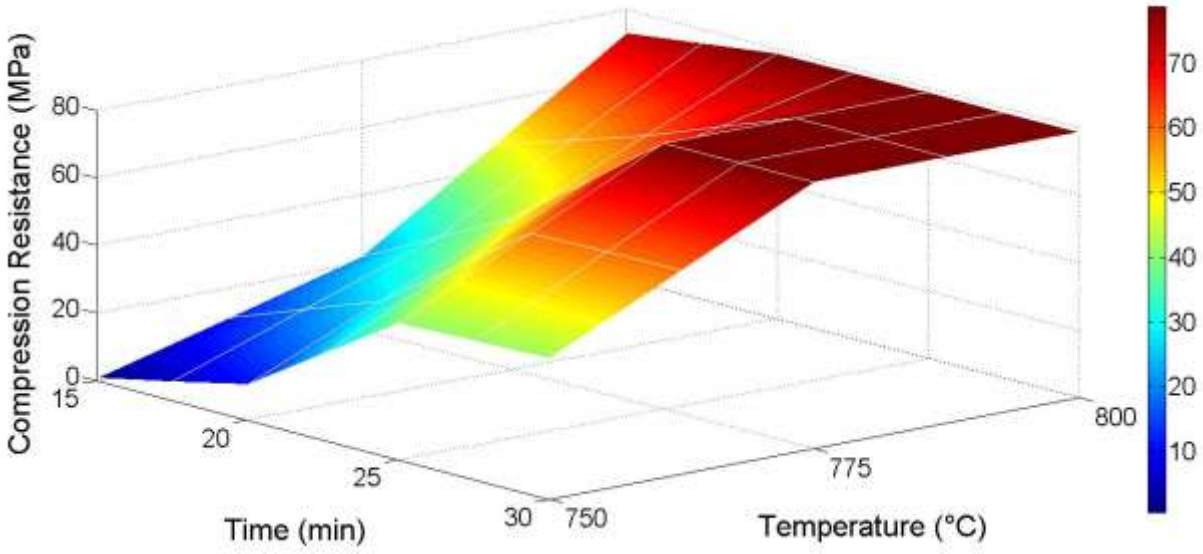

Figure 46: MG80 compressive strength as a function of sintering parameters.

5.1.3.3. MG30 and MG80 Blends

Blends compressive strength decreased by increasing the percentage of MG30. The higher the void size is among particles, the lower the specimen compressive strength becomes. Recalling that voids among MG30 particles are larger than the ones between MG80 particles one can conclude that the addition of MG30 particles increased the amount of voids at samples, which in turn reduced their compressive strength. Figure 47 presents blends compressive strength as function of MG30 percentage. These samples were sintered at 750ºC for 30 minutes because MG30 and MG80 sintered samples presented average porosity and percolation values at this parameters. Equation 16 (R^2 of 97%) is the equation for the fitted model in Figure 47. The error bars presented from 40 to 90 wt% MG30 were due the high particle size distribution of MG30 recycled glass. We have to punctuate that MG30 presents a higher particle size distribution than MG80 recycled glass as explained in section 3.1.3.1.

Equation 16

$$\begin{aligned}\mathbf{Compressive\ Strength}_{\mathbf{MG30+MG80}} &= \mathbf{16.7}\ * \mathbf{exp}\left(\mathbf{-0.08398} * \mathbf{MG30}(\%)\right) \\ &+ \mathbf{24.75} * \mathbf{exp}\left(\mathbf{0.005042} * \mathbf{MG30}(\%)\right)\end{aligned}$$

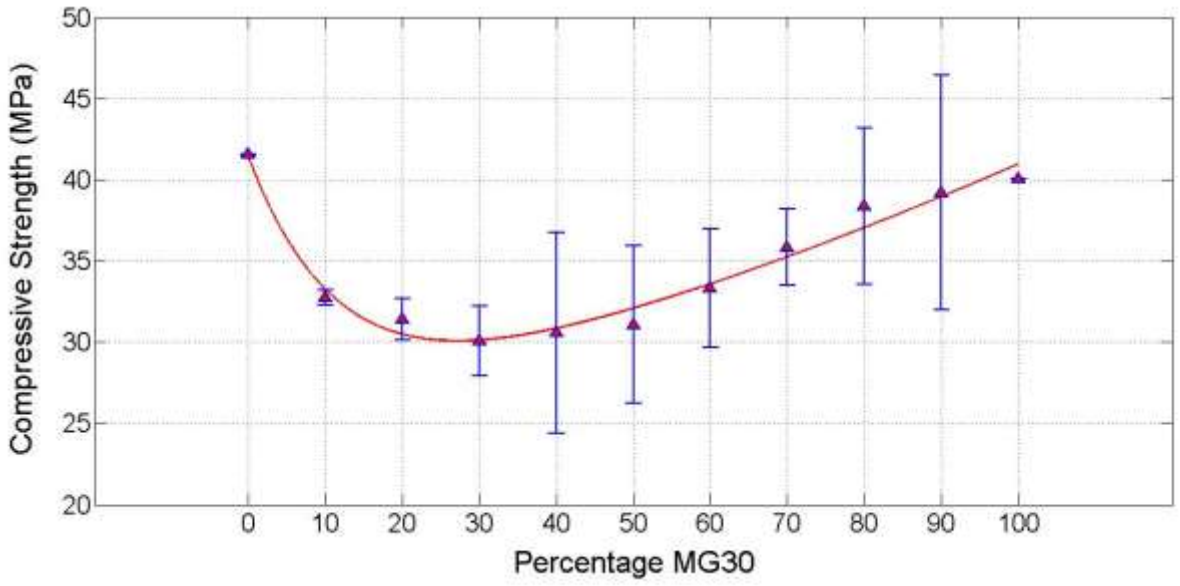

Figure 47: Compressive strength of recycled glass blends as function of MG30 percentage for samples sintered at 750°C for 30 minutes.

5.1.3.4. MG30 with TiO_2 particles

MG30 and TiO_2 anhydrous powder samples were sintered at 800°C for 20 minutes. MG30 compressive strength was decreased by the addition of TiO_2 particles, as shown in Figure 48. The presence of TiO_2 particles decreased the sintering ability of MG30 particles, thus reducing its compressive strength. For concentrations of 0.6 to 1 wt% TiO_2 we can observe a 90% decrease in MG30 compressive strength. This number implies a drastic decrease in the compressive mechanical properties of the material. The presence of TiO_2 in MG30 recycled glass beads impede the complete sintering of

MG30 beads. Equation 17 (R^2=98%) is the equation of the fitted curve of the data shown in Figure 48.

Equation 17

$$\textbf{Compressive Strength}_{\mathbf{MG30+TiO_2}} = \mathbf{205.7} * \mathbf{TiO_2}(\%)^{\mathbf{3}} - \mathbf{254.5} * \mathbf{TiO_2}(\%)^{\mathbf{2}} - \mathbf{20.91} * \mathbf{TiO_2}(\%) + \mathbf{79.87}$$

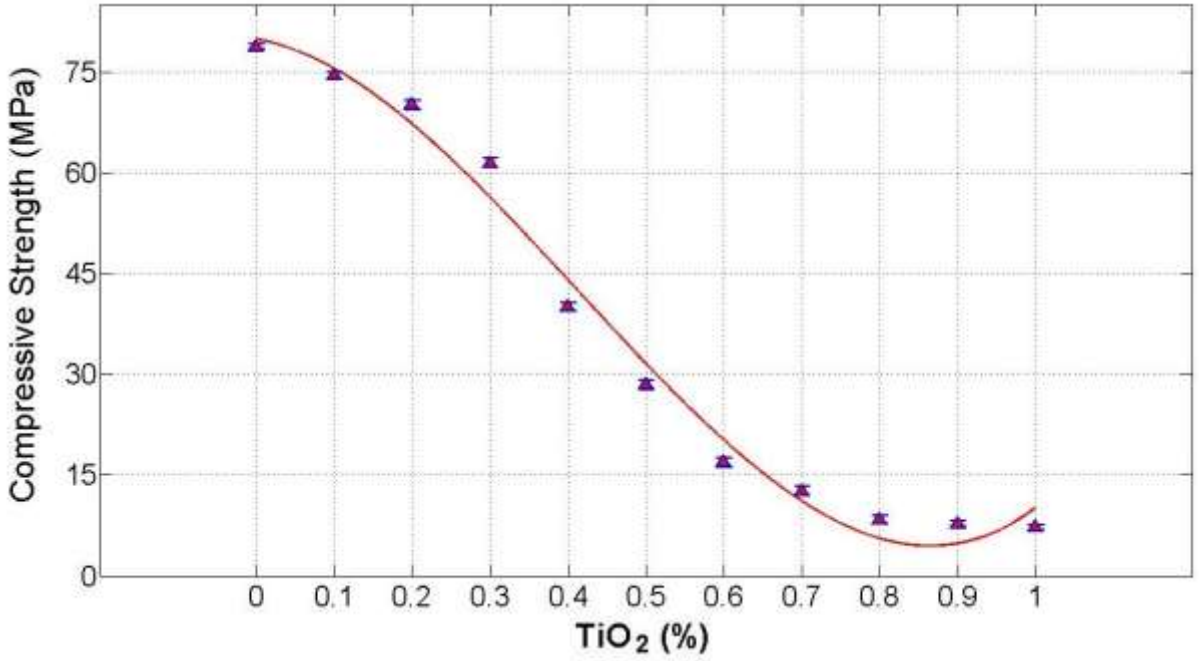

Figure 48: MG30+TiO_2 composites compressive strength as function of TiO_2 percentage.

5.1.3.5. MG80 with TiO_2 particles

Figure 49 shows compressive strength values of MG80 recycled glass sintered with different percentages of TiO_2 anhydrous powder sintered at 800°C for 20 minutes. An exponential behavior is apparent. In this case, TiO_2 particles (average particle size of 12 nm) increase MG80 compressive strength due the decrease of voids in the samples. TiO_2 particles are located between the voids of MG80 particles, which decrease the mobility between MG80 particles. For MG30 recycled glass, TiO_2 particles can't fill the available voids due the big difference between TiO_2 particle size and MG30 voids. Equation 18 (R^2=99%) is the equation of the fitted curve of the data shown in Figure 49.

Equation 18

$$\mathbf{Compressive\ Strength}_{\mathbf{MG80+TiO_2}} = \mathbf{2.801} * \mathbf{exp}\left(\mathbf{-1.867} * \mathbf{TiO_2}(\%)\right) + \mathbf{75.93} * \mathbf{exp}(\mathbf{0.05479} * \mathbf{TiO_2}(\%))$$

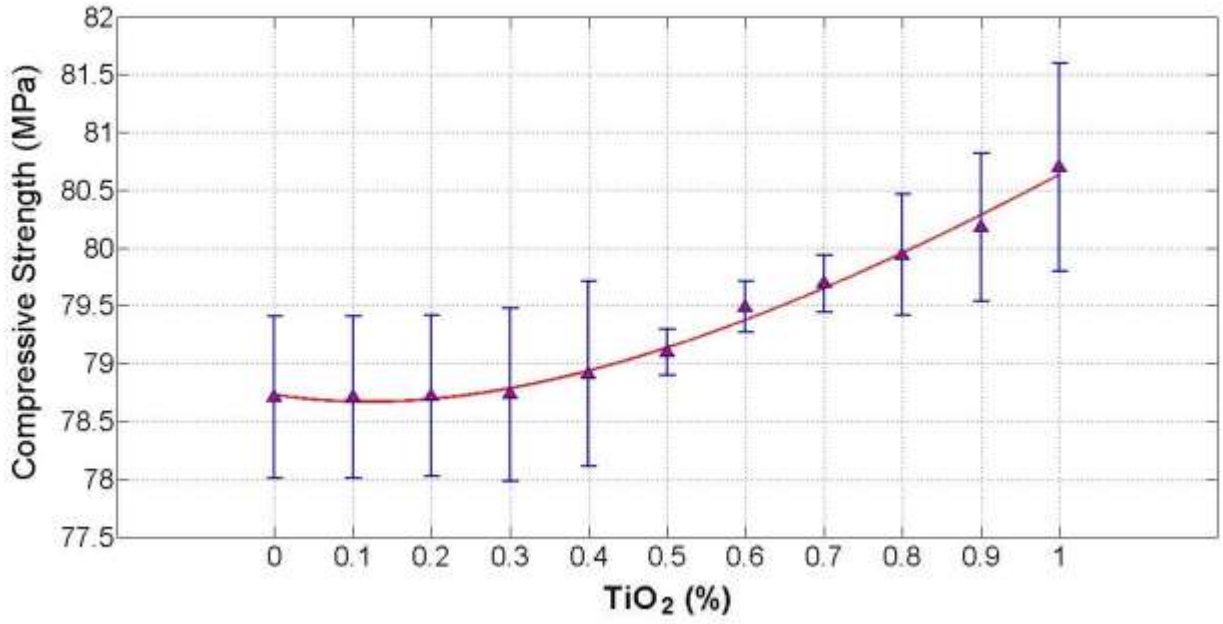

Figure 49: MG80+TiO_2 composites compressive strength as function of TiO_2 percentage.

Conclusions

- We determined the particle size distribution and fineness modulus of MG30 and MG80 recycled glass. Also we described the changes in fineness modulus according to the percentages of MG30 and MG80 present at mixtures.
- We found an inverse relationship between surface porosity and percolation with sintering parameters.
- A direct relationship was found between samples structural parameters with recycled glass particle size. High particle size, delivers high porosity and percolation values, while low particle size delivers lower porosity and percolation values.
- For mixtures, we obtained higher porosity and percolation values for the samples with higher percentage of MG30 particles.
- The addition of low percentages of TiO_2 particles to recycled glass powders, decreased porosity and percolation values due TiO_2 particle size. Moreover, percentages higher of 0.9% TiO_2 decreased recycled glass beads sintering abilities. The recommended sintering parameters for recycled glass and TiO_2 composites were from 750 to 800°C for 20 to 30 minutes (for samples with a total mass of 30 g).
- We found a direct relationship between filters compressive strength and sintering parameters. Furthermore, MG80 recycled compressive strength is higher than the one for MG30 due the small void and particle size.

- Mixtures compressive strength decreased by increasing the percentage of MG30 recycled glass: MG30 increased filters void size thus decreasing its compressive strength.
- The addition of TiO_2 particles decreased the MG30 compressive strength for percentages of 0.5 and 0.6% TiO_2. Moreover, the compressive strength of MG80 recycled glass filters increased by increasing the percentage of TiO_2.
- MG30 and MG80 deformation percentages decreased by increasing sintering parameters. Moreover, samples showed very low deformation percentages at 25°C.
- We were able to increase the distribution of TiO_2 particles across recycled glass beads by increasing beads roughness with phytic acid.

References

1. Ming-Ho, Yu. "Environmental Change and Health." In *Environmental Toxicology*. CRC Press 2004.
2. Rathore, H. S. "Methods of and Problems in Analyzing Pesticide Residues in The Environment." In *Handbook of Pesticides*, 7-46. CRC Press 2009.
3. Pichtel, J. "Recycling Solid Wastes." In *Waste Management Practices,* 136-141. CRC Press 2005.
4. Stellman, J. M., S. D. Stellman, R. Christian, T. Weber, and C. Tomasallo. “The Extent and Patterns of Usage of Agent Orange and other Herbicides in Vietnam.” *Nature* 422, no. 6933, (2003): 681–687.
5. Semple, K. T., B. J. Reid, and T. R. Fermor, “Impact of Composting Strategies on the Treatment of Soils Contaminated with Organic Pollutants.” *Environmental Pollution* 112, no. 2, (2001): 269–283.
6. U.S. Environmental Protection Agency. “*Municipal Solid Waste Generation, Recycling, and Disposal in the United States Tables and Figures for 2010*U. S. Environmental Protection Agency Office of Resource Conservation and Recovery. Accessed June 30, 2013. http://www.epa.gov/osw/nonhaz/municipal/pubs/2010_MSW_Tables_and_Figures_508.pdf

7. “CS Glass Sands.” *Vitrominerals.com*. Accessed June 30, 2013. http://www.vitrominerals.com/wp-content/uploads/CS-Glass-Sand-TDS-100805.pdf Nov. 2010.
8. Luigi, R., “Granulometry.” In Materials Laboratory Manual of Civil Engineering, (1999): 10-21.
9. Umar, M., and H. A. Aziz, “Photocatalytic Degradation of Organic Pollutants in Water.” *Intechopen.com,* Accessed June 30, 2013. http://www.intechopen.com/books/organic-pollutants-monitoring-risk-and-treatment/photocatalytic-degradation-of-organic-pollutants-in-water
10. Wang, M., J. Yan, H. Cui, and S. Du, “Low Temperature Preparation and Characterization of TiO_2 Nanoparticles Coated Glass Beads by Heterogeneous Nucleation Method.” *Materials Characterization* 76, no. 97, (2012): 39–47.
11. McNaughton, A. L. “High Temperature Compression Testing of Monolithic Silicon Carbide (SiC).” Master's thesis, University of Maine, 2007. https://www.library.umaine.edu/theses/pdf/McNaughtonAL2007.pdf
12. Holtz, R. D and W.D. Kovacs, “The Unified Soil Classification System (USCS).” In *An Introduction to Geotechnical Engineering*, 49-64. Englewood Cliffs, NJ:Prentice Hall, 1981.
13. LaGrega, M. D., P. L. Buckingham, and J.C. Evans. “Water Remediation.” In *Hazardous Waste Management*, 156-190. Boston, MA: McGraw-Hill, 2001.
14. Lobbestael, A. and E. Wild. “Soil Vapor Extraction.” *Geoengineer.org*. Accessed June 30, 2013. http://www.geoengineer.org/education/web-based-class-

projects/geoenvironmental-remediation-technologies/vapor-extrusion?showall=&start=1

15. U.S. Environmental Protection Agency. "*Chapter VII Air Sparging*. *Epa.gov."* Accessed June 30, 2013. http://www.epa.gov/oust/pubs/tum_ch7.pdfU.S.
16. U.S. Environmental Protection Agency. *"Soil/Sediment Washing System*. Bergman USA: Demonstration Bulletin (EPA 540-MR-92-075).
17. LaGrega, M. D., P. L. Buckingham, and J. C. Evans. "Permeable Reactive Treatment Walls." In *Hazardous Waste Management*, 1037-1040. Boston, MA: McGraw-Hill, 2001.
18. LaGrega, M. D., P. L. Buckingham, and J. C. Evans. "Pump-and-Treat.", In *Hazardous Waste Management*, 1013-1017. Boston, MA: McGraw-Hill, 2001.
19. LaGrega, M. D., P. L. Buckingham, and J. C. Evans. "Air Sparging." In *Hazardous Waste Management*, 1017-1019. Boston, MA: McGraw-Hill, 2001.
20. LaGrega, M. D., P. L. Buckingham, and J. C. Evans, "Degradation Treatment Walls.", In *Hazardous Waste Management*, 1040-1044. Boston, MA: McGraw-Hill, 2001.
21. Cullity, B. D. and S. R. Stock. "Crystallite Size." In *Elements of X-Ray Diffraction*, 169-170. Upper Saddle River, NJ: Prentice Hall, 2001.

22. Fox, M. A. and M.T. Dulay. “Heterogeneous Photocatalysis.” *Chemical Reviews* 93, no. 1, (1993): 341-353.
23. Rajeshwar, K., and J. Ibáñez. “Environmental Electrochemistry.” In *Fundamentals and Fundaments in Pollution Abatement*. SD: Academic Press, 2007.
24. Mandelbaum, P., A. Regazzoni, M. Belsa, and S. Bilme, “Photo-electron-oxidation of Alcohol on Titanium Dioxide Thin Film Electrodes.” *Journal of Physics and Chemistry*, (1999): 5505-5511.
25. Ahmed, S., M. G. Rasul, R. Brown, and M. A. Hashibi, “Influence of parameters on the Heterogenous Photocatalytic Degradation of Pesticides and Phenolic Contaminats in Wastewater: A Short Review.” *Journal of Environmental Management*, (2011):311-330.
26. Rahaman, M. N., "Sintering of Ceramics: Fundamentals." In *Sintering of Ceramics*, 1-2. CRC Press, 2008.
27. Rahaman, M. N., "Solid-State and Viscous Sintering." In *Sintering of Ceramics*, 45-47. CRC Press, 2008.
28. Rahaman, M. N., "Grain Growth in Very Porous Solids." In *Sintering of Ceramics*, 153-154. CRC Press, 2008.